Integrating outcomes from probabilistic and deterministic approaches for seismic hazard assessment in the Northern Tien Shan region

I. Mosca[1], B. Baptie [1], S. Sargeant [1], R. T Walker [2]

[1] British Geological Survey, the Lyell Centre, Research Avenue South, Edinburgh EH14 4AP, United Kingdom

[2] COMET, Department of Earth Sciences, Oxford University, South Parks Road, Oxford OX1 3AN, United Kingdom

Abstract (Max 250 words)

Seismic hazard can be assessed either probabilistically or deterministically. Probabilistic seismic hazard assessment (PSHA) and deterministic seismic hazard assessment (DSHA) are usually used independently, with the former often preferred in engineering and reinsurance applications. The latter is an appropriate tool for stakeholders engaged in policy-making and community-based risk reduction activities.

The Tien Shan mountain belt (Central Asia) is a low strain rate environment within the interior of a continent where large earthquakes are infrequent and are associated with long (up to thousands of years) recurrence intervals. This means that there is a limited amount of seismic data to assess seismic hazard in a robust way. For this reason, the Northern Tien Shan is the ideal candidate to apply an approach that integrates the outcomes from PSHA and

DSHA to overcome their individual limitations and the lack of extensive seismological and geological records in the area.

The focus of this study is Almaty, the former capital of Kazakhstan and the largest city in the region. First, taking a deterministic approach, we simulate ground shaking scenarios for three destructive historical earthquakes that occurred in the Northern Tien Shan in 1887, 1889 and 1911, using ground motion prediction equations and realistic (although simplified) fault rupture models based on recent geomorphological and paleoseismological studies. We show that the large variability in the ground motion prediction equations results in large uncertainty in the ground motion simulations.

Then, taking a probabilistic approach, we estimate the seismic hazard for the same site using Monte Carlo simulations. The PSHA is based on an earthquake catalogue compiled from the databases of the International Seismological Centre and the British Geological Survey. From this analysis, we show that the seismic hazard of Almaty is strongly influenced by earthquakes with $7.0 \leq Mw \leq 7.8$ relatively close (< 30 km) to the city.

Introduction

Seismic hazard can be assessed using either the probabilistic seismic hazard analysis (PSHA) (e.g. for review see Reiter, 1990; McGuire, 2004; Abrahamson, 2000; Bommer et al., 2005) or the deterministic seismic hazard analysis (DSHA) (e.g. for reviews see Reiter, 1990; Kramer, 1996). Their use depends on several factors including the purpose of the assessment (i.e. how quantitative the decisions to be made are), the seismic environment (if it is high, medium or low hazard), and the scope of the project (i.e. whether it is for a single site or a region) (e.g. McGuire, 2001; Gupta, 2002; Klügel, 2008).

Strengths and weaknesses of PSHA and DSHA have been discussed by many authors (e.g. Reiter, 1990; McGuire, 2004; Abrahamson, 2006) and here we summarize them briefly. The strength of PSHA is the integration of a wide range of information and the inclusion of the uncertainties associated with the input parameters (e.g., earthquake sources, seismic path, soil conditions and ground shaking) into a probabilistic framework to determine the frequency with which different levels of ground motions occur. However, this can also be seen as a limitation because the hazard results expressed in probabilistic terms may not be easily understood by non-specialists. A second limitation of PSHA is that it may be difficult to understand how each input parameter affects the result because it accounts for all uncertainties in a probabilistic framework. For this reason, PSHA has been criticized as a mere mathematical procedure with little connection to the earthquake physics, especially for hazard results at long return periods (see discussion in Krinitzsky, 2003; Klügel, 2005; and Wang and Cobb, 2012). The strengths of DSHA are the relatively simple procedure it uses, and the clear relationship between the seismic source (i.e. the earthquake) and the potential hazard (i.e. the ground shaking). However, DSHA has a significant limitation. The method

58 lacks any probabilistic dimension because the earthquake recurrence and the chance of
59 exceeding the design ground motion are not addressed directly (Abrahamson, 2006).

60 In this paper, following the recommendations of Reiter (1990), McGuire (2001) and Aspinall
61 (2013), we combine the outcomes from PSHA and DSHA to reduce their limitations. This
62 integrative approach is highly recommended for critical infrastructures, such as dams
63 (ICOLD, 2010) and nuclear power plants (IAEA, 2010). We evaluate the deterministic
64 scenarios within a probabilistic framework to estimate the annual probability of exceedance
65 of the deterministic value(s). We also check the probabilistic analysis with DSHA to
66 determine the earthquake scenario for low annual probabilities of exceedance. In this way, we
67 ensure that PSHA is not a mere mathematical formalism but is connected to the earthquake
68 physics (Reiter, 1990; McGuire, 2001; Aspinall, 2013).

69 We apply the integrative approach of PSHA and DSHA to the Tien Shan region, which is
70 situated in a low strain region in the interior of the Eurasian plate (e.g. Landgraf et al., 2016).
71 In the Tien Shan large (Mw > 7) earthquakes are infrequent and their recurrence interval is
72 long (up to thousands of years) because the slip is accumulated slowly (rates of less than one
73 millimetre per year), compared to the slip rate along plate boundaries, i.e. 10-100 mm/yr.
74 (England and Jackson, 2011). This makes a robust seismic hazard assessment challenging
75 because the observed catalogue may not adequately reflect the long-term earthquake history
76 (e.g. Abdrakhmatov et al., 2016; Landgraf et al., 2016). As a result, using only PSHA or
77 DSHA independently of each other may be insufficient for the Northern Tien Shan. Instead,
78 integrating the outcome from PSHA and DSHA may produce a more rigorous seismic hazard
79 assessment. The focus of the present work is Almaty, the former capital of Kazakhstan and
80 the largest city in the region. The city is situated in a depression at the foothill of the Alatau
81 mountain ranges (Pilz et al., 2015), which are marked by poorly understood and often

unknown faults before an earthquake occurs along them. At the beginning of last century the population of Almaty was a few thousands of people, but after the collapse of the Soviet Union the population has grown up to almost two millions, making the city more vulnerable.

Recent studies have mapped and characterised the probable surface ruptures associated with the historical earthquakes that occurred between 1885 and 1911 in the Northern Tien Shan (e.g. Arrowsmith et al., 2016; Abdrakhmatov et al., 2016). They allow us to simulate the ground shaking based on realistic fault rupture models using DSHA. We provide a frequency of occurrence for the seismicity in the Northern Tien Shan, using the recurrence statistics and the earthquake catalogue in the Northern Tien Shan. Finally, we apply PSHA to determine return periods (i.e. the inverse of the annual probability of exceedance) of different levels of the ground shaking for a site in Almaty. The hazard results obtained from PSHA are disaggregated to show the contribution of future earthquakes similar to the earthquakes, which occurred between 1887 and 1911, to the overall hazard of Almaty.

Regional setting

The Tien Shan is a tectonically and seismically active intraplate mountain belt that is bounded by the Kyzyl-Kum desert to the east and the Gobi Desert to the west, and lies between the Kazakh Platform to the north and the Tarim Basin to the south (Figure 1). It is ~2500 km long, with peaks up to ~7400 m high and widens from east to west, reaching a maximum of ~400 km width (Figure 1).

The formation of this mountain belt is a consequence of the continental collision between the Indian and Eurasian plates that started ~50 Ma ago. This resulted in the re-activation of Pre-Cenozoic structures in the last 50 Ma ago in Central Asia, including the Tien Shan, (e.g.

Tapponnier and Molnar, 1979; Burtman et al., 1996; Paul et al., 2001). The present-day crustal shortening across the Tien Shan is ~20 mm/yr., corresponding to 40% of the crustal shortening between India and Eurasia, even though the mountain belt is situated more than 1000 km north of the boundary (DeMets et al., 1990; Abdrakhmatov et al., 1996; Reigber et al., 2001; Zubovich et al., 2010; Campbell et al., 2013). This deformation is accommodated by E-W oriented thrusts, NNW-SSE-trending right-lateral strike-slip faults, and ENE-WSW-trending left-lateral strike-slip faults (e.g. Tapponnier and Molnar, 1979; Thompson et al., 2002; Abdrakhmatov et al., 2016). The E-W-striking faults delineate the E-W-trending mountain ranges and the sub-parallel intra-mountain basins (Tapponnier and Molnar, 1979; Bullen et al., 2001; Thompson et al., 2002). The major strike-slip structure in the Northern Tien Shan is the NNW-SSE oriented right-lateral strike-slip Talas-Ferghana Fault. It accommodates part of the N-S shortening in the Tien Shan with different rate of convergence between the western and eastern Tien Shan (Alinaghi and Krüger, 2014; Campbell et al., 2013).

SEISMICITY IN THE NORTHEN TIEN-SHAN

The seismicity in the Tien Shan mountain belt is characterized by a large number of earthquakes with Mw < 7 and a small number of large (Mw ≥ 7) events. Indeed, there have not been any very large (Mw > 8) earthquakes in this area since the beginning of the 20th century. Since the slip is accumulated slowly in a low strain rate environment, the recurrence interval of large earthquakes on active faults in the Tien Shan is likely to exceed the length of historical earthquake records and so the seismicity catalogue presents an incomplete picture of the earthquake environment (e.g. Abdrakhmatov et al., 2016; Landgraf et al., 2016), which will have implications for an assessment of seismic hazard. Furthermore, the faults on which

such large earthquakes occur often go unidentified until an event occurs, as was the case for the 2010 Canterbury (New Zealand) earthquake (e.g. Landgraf et al., 2016).

The seismicity in the Tien Shan is associated with faults bounding the intra-mountain basins (e.g. Lake Issyk-Kul and the Ferghana Basin) and tend not to occur within the basins (Figure 1) (Zubovich et al., 2010; Alinaghi and Krüger, 2014). The largest historical earthquakes in the region have been recorded along the northern (i.e., 6.9 Ms 1885 Belovodsk; 7.3 Ms 1887 Verny; 8.3 Ms 1889 Chilik; 8.0 Ms 1911 Chon-Kemin) and southern margins of the Tien Shan (e.g. 8.0 Ms 1902 Artux). High levels of instrumental seismicity (considered here to be earthquakes that have occurred since 1964) with magnitude smaller than 7.0 are recorded along the margin between the Tien Shan and the Tarim Basin and to a lesser extent, along the margin between the Tien Shan and the Kazakh Platform (Alinaghi and Krüger, 2014) (Figure 1). The largest of these are the 7.3 Ms 19 August 1992 Suusamyr earthquake and the 6.9 Mw 24 March 1978 Dzhalanash-Tyup earthquake, which were both situated in the Northern Tien Shan (Figure 1). It is worth noting that the 1992 Suusamyr earthquake, together with its sequence of aftershocks, is the first well-recorded seismic sequence in the region (Ghose et al., 1997; Mellors et al., 1997). It nucleated on a reverse fault at a depth of ~20 km (Molnar and Ghose, 2000). It produced only ~4 km long surface ruptures near the western end of the fault rupture that was inferred from the aftershocks and a further ~0.5 km long surface rupture at the eastern end (Ghose et al., 1997; Mellors et al., 1997). It is therefore likely that much of the seismic rupture failed to reach the surface (Ghose et al., 1997; Mellors et al., 1997).

Moderate ($Mw < 6$) levels of seismicity are associated with the Talas-Ferghana fault and no major ($Mw > 7.0$) earthquakes have occurred along this fault in the last 200 years (Campbell et al., 2013).

The general tectonic regime in the Tien Shan is compressional and the dominant focal mechanism is reverse faulting with various degree of strike-slip component (Alinaghi and Krüger, 2014). The P-axis of focal mechanism of the earthquakes in the region is oriented N-S, in agreement with the direction of the convergence between India and Eurasia (e.g. Tapponnier and Molnar, 1979; Alinaghi and Krüger, 2014). There are also a few strike-slip events, e.g. the 6.3 Mw 12 November 1990 earthquake and the 6.2 Mw 28 January 2013 earthquake.

Sloan et al. (2011) used inversion of teleseismic body waves, identification of depth phases and modelling of regional waveforms, to relocate 123 earthquakes with Mw ≥ 5.2 in the Tien Shan region. They find that focal depths for earthquakes in the Tien Shan mountain belt are in the upper crust at depths of less than 30 km; whereas, the earthquakes in the Tien Shan Foreland, including the Kazakh Platform and the Tarim Basin, are observed in the mid and lower crust to depths of 40 km, suggesting a greater seismogenic thickness. This may suggest the presence of remnants of subducting plate or underplating involved in the formation of the Tien Shan (Alinaghi and Krüger, 2014).

RECURRENCE STATISTICS IN THE NORTHEN TIEN-SHAN

To determine the frequency of occurrence for the seismicity in the Northern Tien Shan, we use the Gutenberg-Richter recurrence law (Gutenberg and Richter, 1954) and the earthquake catalogue in the Northern Tien Shan.

The earthquake catalogue consists of data from three sources for the region bounded by 39°-46°N and 70°-81°E and the time period from 205 BC to 31 October 2013 (Figure 1). The event sources are: the International Seismological Centre Bulletin; the World Seismicity Database (WSD) of the British Geological Survey (Henni et al., 1998); and the earthquake

174 catalogue for the "Earthquake Model for Central Asia" (EMCA) project (Mikhailova et al.,
175 2015). See Appendix for more information about the preparation of the earthquake catalogue.

176 The recurrence statistics is given by the Gutenberg-Richter law that expresses the relationship
177 between the magnitude and number of earthquakes in a given region and time period
178 (Gutenberg and Richter, 1954):

179 $$\text{Log } N = a - b\,M \qquad (1)$$

180 Where N is the number of earthquakes above a given magnitude M. The activity rate, *a*,
181 describes the total number of earthquakes per year in the study area, and the *b*-value gives the
182 proportion of large events to small ones. In general, *b*-values tend to be close to one (e.g.
183 Reiter, 1990).

184 To maximize the information in the earthquake catalogue, we applied a penalized maximum
185 likelihood procedure (e.g. Johnston et al., 1994) to determine both the activity rate, *a*, and the
186 *b*-value. This procedure uses the truncated Gutenberg-Richter recurrence law where the
187 earthquake magnitudes are bounded by lower and upper bounds. We used a correction factor
188 in the activity rate calculations based on the standard error of individual earthquake
189 magnitudes, as proposed by Rhoades and Dowrick (2000). A number of authors, including
190 Tinti and Mulargia (1985), Rhoades (1996), Rhoades and Dowrick (2000) and Castellaro et
191 al. (2006), have shown that ignoring uncertainty in the magnitude values results in an
192 overestimation of the seismicity. We assume that all magnitude values in the catalogue have
193 an uncertainty of ± 0.2 that corresponds to the standard deviation in the magnitude
194 conversion equations of Scordilis (2006). This uncertainty may be small for historical events
195 in the Tien Shan, as suggested by Zöller at al. (2017) who use $\sigma = \pm 0.5$ for historical events,
196 $\sigma = \pm 0.25$ for early instrumental events and $\sigma = \pm 0.1$ for recent instrumental recorded events

in Central Asia. We decided not to use these values since it is not clear how these are estimated. Musson (2012b) shows that the magnitude uncertainty should be used carefully to avoid over- or under-estimation of the seismicity in the area, especially when the earthquake catalogue merges many sources and contains more than one original magnitude scale.

Equation (1) was applied to all the seismicity in the study area, using the maximum likelihood method and the completeness thresholds discussed in Appendix. The best- fit values for equation (1) are $N\,(\mathrm{Mw} \geq 4.5) = 28.19 \pm 0.72$ for and $b = 0.959 \pm 0.020$ (Figure 2). The values give a credible fit to the data, which might reasonably be supposed to be complete. The error-bars in Figure 2 describe the uncertainties in the data points as expressions of the long-term recurrence of that magnitude value and is inversely proportional to the number of observations in the catalogue.

Mikhailova et al. (2015) have found a *b*-value of 0.805 for the entire Central Asia (i.e. 34°-56°N, and 47.5°- 90°E) that is smaller than the estimated *b*-value in this work. The difference between the two values may be explained by three reasons. First, we applied equation (1) to a smaller region (i.e. 39°-46°N and 70°-81°E) than the entire Central Asia. Second, the earthquakes in our catalogue are expressed in Mw, and not the surface wave magnitude according to the Moscow-Prague formula (Karnik, 1962) M_{LH} as in the earthquake catalogue of Mikhailova et al. (2015). Therefore, different magnitude conversion equations were applied to homogenize the two catalogues. Third, the magnitude completeness of the two catalogues is different for Mw < 5.5.

Deterministic approach

DSHA is generally based on discrete, single-valued models to arrive at scenario-like descriptions of seismic hazard, using geological data and searching for active faults (Reiter,

1990). After defining the seismic source(s) (fault or large seismotectonic area) in the study area, the controlling earthquake that usually is the largest earthquake that the seismic source is capable of generating is selected. How the magnitude of the controlling earthquake is defined will determine the level of conservatism of the assessment (Reiter, 1990). The level of ground shaking (i.e. peak ground acceleration -PGA-, peak ground velocity -PGV-, spectral acceleration, and intensity) at the site caused by the controlling earthquake is estimated using a ground motion prediction equation (GMPE) or a numerical method to simulate the ground motion.

For each earthquake rupture model and GMPE, we compute a set of values for the selected ground motion parameter (e.g. PGA and spectral acceleration) for a single site or grid point. We model the earthquake assuming the slip is homogeneous and using a simple 3D finite fault rupture that is described by the fault orientation (i.e. strike, dip and rake), the depth to which the fault extends (i.e. thickness of the seismogenic zone), the rupture aspect ratio (the ratio between length and down-dip width of the fault rupture) and a magnitude-length scaling relationship. We compute the ground shaking for the controlling earthquakes using GMPEs rather than a numerical approach as the latter requires many parameters (e.g. attenuation model, slip or stress model, rupture velocity, and source duration) that are poorly constrained or unknown for the historical earthquakes in the Tien Shan, which would greatly increase the uncertainty in the results. By contrast, the GMPEs used in this study were derived from large worldwide strong motion datasets, and are considered appropriate for the tectonic regime of the Tien Shan, i.e. active shallow crustal regime.

For the controlling earthquake, its rupture model, one or more selected GMPEs and a specific site, the ground motion value is computed using Monte Carlo simulations (i.e. controlled generator of random numbers). This procedure allows us to include uncertainties in the input

parameters by drawing parameter values within their probability density functions (*pdf*s), defined by observed mean and standard deviation. Multiple earthquake scenarios can be computed, each sampling the uncertainty in the input parameters. For the GMPE, the *pdf* is represented by the median prediction of the GMPE for the particular distance and magnitude of the controlling earthquake within one standard deviation (1σ) of the ground motion model, i.e. the aleatory uncertainty of the GMPE. The deterministic approach traditionally uses 1σ around the median prediction for the GMPEs, which corresponds to the 84th percentile ground motion (e.g. Abrahamson, 2006).

DEFINING THE SCENARIO EARTHQUAKES

In this study, we use the deterministic analysis to simulate the ground motion scenario for the three largest earthquakes recorded in the Northern Tien Shan region between the end of the 19th century and the beginning of the 20th century, i.e. the 7.3 Ms 1887 Verny earthquake; the 8.3 Ms 1889 Chilik earthquake; and the 8.0 Ms 1911 Chon-Kemin earthquake (Figure 1). All of them resulted in badly damaging Almaty. There is no evidence that these earthquakes are the closest and largest potential earthquakes to Almaty due to the short length of the earthquake catalogue in the region (see Appendix). Therefore, we refer to them not as controlling earthquakes, but as scenario earthquakes.

For each of these earthquakes, we determine the rupture geometry based on the available information in the literature, geological observations and earthquake physics. We use: 1) the self-consistent (i.e. all the variables can be estimated from each other) empirical relationships of Leonard (2010) derived from a large worldwide earthquake database, to estimate the dimension of the fault rupture using the moment magnitude; and 2) the definitions of seismic moment M_0 (Aki, 1966) and moment magnitude (Kanamori, 1977; Hanks and Kanamori,

1979) to estimate M_0 and the average slip for a shear modulus of 3.3×10^{10} N/m^2, i.e. typical value for crustal faults (e.g. Molnar & Ghose, 2000; Stein & Wysession, 2003).

The parameters of the reference rupture model of the three scenario earthquakes are summarized in Table 1, together with their uncertainty if available from published sources or estimated from the propagation of statistical errors. The location of the epicenters and the length of the fault ruptures are shown in Figure 3.

1887 Verny earthquake

The 8 June 1887 Verny earthquake was the closest event of the sequence to Almaty and the epicenter was located ~30 km west of the city. One month after the event, an expedition was sent from St. Petersburg into the epicentral area to collect macroseismic information (Mushketov, 1890). These macroseismic data were used to infer the surface wave magnitude of the earthquake, estimated to be 7.3 M_{LH}, i.e. surface wave magnitude according to the Moscow-Prague formula of Karnik (1962) (Mushketov, 1890; Tatevossian, 2007; Bindi et al., 2014). Kondorskaya and Shebalin (1982) also use the macroseismic data to estimate isoseismals for the earthquake and use this to determine a focal depth of 20 km, a surface wave magnitude of 7.3 ± 0.5 M_{LH} and an epicentral intensity of I_0 = (IX-X) ± 0.5. Tatevossian (2007) use coseismic environmental effects to determine a magnitude between 7.3 and 7.5. Using the conversion equation of Scordilis (2006), 7.3 Ms corresponds to 7.3 ± 0.2 Mw (Table 1) and the associated seismic moment is 1.0×10^{20} Nm.

No surface rupture has been identified for this earthquake, potentially because the event triggered many large landslides that may have covered the fault trace (Abdrakhmatov et al., 2016). For this reason, very little is known about the rupture process of this event.

289 Using the length-magnitude scaling relationships of Leonard (2010), an earthquake of 7.3 ±
290 0.2 Mw generates a 75 ± 20 km long and 31 ± 8 km wide rupture (Table 1). The average
291 displacement is 1.3 m from the Aki (1966) equation relating seismic moment to shear
292 modulus, displacement and rupture size.

293 We assume a reverse faulting mechanism with a small strike-slip component, similar to the
294 mechanism of the 1911 earthquake (Table 1). However, a pure reverse focal mechanism, in
295 agreement with focal mechanisms determined for other earthquakes in the Zailisky Alatau
296 range, cannot be ruled out.

297 **1889 Chilik earthquake**

298 The 11 July 1889 Chilik earthquake is one of the largest historical continental events in the
299 world and one of the earliest teleseismically recorded earthquakes (Krüger et al., 2016).
300 Despite its size, relatively little is known about the source of the earthquake because the
301 isoseismals were derived by questionnaires sent out by the Russian Geographical Society in
302 St. Petersburg to the epicentral area after the event (Mushketov, 1891). Mushketov (1891) do
303 not report any primary surface rupture and assign a MSK-64 intensity of IX-X around the
304 Chilik River and VII-VIII in Almaty (Figure 4). Kondorskaia et al. (1982) and Besstrashnov
305 (1993) estimate a magnitude of 8.3 M_{LH} based on macroseismic observations. Bindi et al.
306 (2014) give a magnitude of 8.3 Ms using the data from the earthquake catalogue of
307 Mikhailova et al. (2015). Krüger et al. (2016) estimate Mw to be between 8.0 and 8.3 with a
308 preferred value of 8.0 by analyzing a fragment of an early Rebeur-Paschwitz seismometer,
309 recorded in Wilhelmshaven (Germany), and magnetograph readings for the earthquake. We
310 assume the moment magnitude for this earthquake to be 8.2 Mw, an average value between
311 the findings of Krüger et al. (2016) and Bindi et al. (2014), with an uncertainty of 0.2, i.e. the

312 standard deviation in the magnitude conversion equations of Scordilis (2006) (Table 1). A 8.2
313 Mw value corresponds to a scalar seismic moment of 2.23×10^{21} Nm.

314 The Chilik earthquake was associated with the E-W trending left-lateral Chon-Kemin-Chilik
315 fault zone (Abdrakhmatov et al., 2002; Buslov et al., 2003; Krüger et al., 2016;
316 Abdrakhmatov et al., 2016). The epicenter location is not well constrained by the intensity
317 observations in Mushketov (1891) and has an uncertainty of 0.5º (Kondorskaya and Shebalin,
318 1982; Bindi et al., 2014).

319 Recent field investigations have found evidence of fresh scarps that may be associated with
320 the Chilik earthquake (Tibaldi et al., 1997; Crosby et al., 2007; Abdrakhmatov et al, 2016).
321 Abdrakhmatov et al. (2016) identify three segments that potentially ruptured during this
322 event: the 45-km right-lateral Beshkaragai segment; the 30-km Saty segment with an oblique
323 left-lateral slip; the 100-km right-lateral Kurmentey segment (Figure 3). They sum up to a
324 total of 175-km of complex multi-segmented surface rupture including step-overs (up to 6-7
325 km) (Abdrakhmatov et al, 2016). Using the length-magnitude scaling relationships of
326 Leonard (2010), an earthquake of 8.2 ± 0.2 Mw would be associated with a 260 ± 71 km long
327 rupture.

328 The focal depth of this seismic event cannot be constrained with the available data. Bindi et
329 al. (2014) and Krüger et al. (2016) suggest a hypocentral depth in the mid or lower crust. A
330 potential depth of 40 km may be consistent also with the broad isoseismals of this earthquake
331 (Figure 4). However, this hypothesis is not supported by any geological evidence. Therefore,
332 a smaller (~ 20-25 km) depth cannot be ruled out, as discussed in Krüger et al. (2016) and
333 Sloan et al. (2011).

Since the focal depth is unconstrained, the geometrical extent of the fault plane is unknown. However, we fix the vertical depth of the fault plane to 40 km, based on Sloan et al. (2011), which suggest that the seismogenic layer is 40 km thick. We did not use the scaling relationship to evaluate the down-dip width of the fault rupture because the thickness of the seismogenic layer limits the rupture width, especially for large strike-slip earthquakes (e.g. Stock and Smith, 2000; Leonard, 2010). A 40 km vertical depth of the fault plane agrees well with the recent seismicity in the region that occurs in the first 30 km of the crust, as supported by the source parameters of the 1992 Suusamyr earthquake (Mellors et al., 1997; Sloan et al., 2011; Alinaghi and Krüger, 2014). The hypocenters of this event and its sequence of aftershocks have focal depths between the surface and 18 km depth (Mellors et al., 1997).

The focal mechanism of the 1889 earthquake determined from geological observations favors oblique faulting with a large strike-slip component (Abdrakhmatov et al., 2016; Krüger et al., 2016). Therefore, we assume a dip of 70° (Table 1).

1911 Chon-Kemin earthquake

The 8.0 Ms 3 January 1911 Chon-Kemin (or Kebin) earthquake caused a relatively low number of casualties considering its size because the region was sparsely populated at the beginning of the 20th century (e.g. Abdrakhmatov et al., 2002; Buslov et al., 2003; Kulikova and Krüger, 2015). A field expedition was sent to the epicentral area three months after the event to investigate the damage from the earthquake (Bogdanovich et al., 1914). Bogdanovich et al. (1914) assign a MSK-64 intensity of X in the epicentral zone and VIII in Almaty (Figure 4).

The earthquake has been studied by various authors, resulting in a number of different estimates of the epicentre and magnitude. Abdrakhmatov et al. (2002) and Buslov et al. (2003) report a surface wave magnitude of 8.2. Arrowsmith et al. (2016) infer 7.9 Mw from

geological observations. Finally, Kulikova and Krüger (2015) estimate that the size of the Chon-Kemin earthquake is Mw = 8.02 ± 0.10 comparing observed and synthetic seismograms. The seismic moment for an earthquake of 8.02 ± 0.10 Mw is 1.20 $x10^{21}$ Nm.

Bogdanovich et al. (1914) estimate that the epicenter was situated near the junction between the Chon-Kemin, Chilik and Chon-Aksu valleys (Figure 3). The historical catalogues of Gutenberg and Richter (1954), Kondorskaya and Shebalin (1977), Abe and Noguchi (1983) and Storchak et al. (2013) all report different epicentral locations with an uncertainty of 1° in longitude and <1° in latitude (Kulikova and Krüger, 2015). For example, Molnar and Ghose (2000) report the epicenter at 42.8°N and 77.3°E. Kulikova and Krüger (2015) use digitized data from 23 seismic stations worldwide to relocate the epicenter at 42.996 ± 0.279°N and 77.367 ± 0.494°E.

The Chon-Kemin earthquake produced a total of 145-195 km rupture on six different fault segments of the Chon-Kemin-Chilik fault (e.g. Molnar and Ghose, 2000; Abdrakhmatov et al., 2002; Kulikova and Krüger, 2015; Abdrakhmatov et al., 2016). Applying the scaling relationships of Leonard (2010), we estimate that an earthquake of 8.02 ± 0.10 Mw generates a rupture of 202 ± 28 km length. We fix the vertical extent of the Chon-Kemin fault plane to 40 km following the same reasoning as described for the Chilik earthquake. However, it is worth noticing that the focal depth for the Chon-Kemin event derived from the waveforms is 20 ± 3 km (Kulikova and Krüger, 2015), and not 40 km as for the Chilik event. This means that although the two earthquakes have the same vertical fault width, the 1911 earthquake is shallower. This is supported by the trend of the isoseismals that are broader for the 1889 earthquake than for the 1911 earthquake, indicating a deeper hypocentre in the first case (Figure 4). Assuming a shear modulus of 3.3x10^{10} N/m^2, a ruptured area of 202 km length

and 50 km down-dip width, and M_0=1.20x10^{21} Nm, the average slip is ~3.6 m, in agreement with the estimate of Molnar and Ghose (2000), i.e. 4.0 ± 1.5 m (Table 1).

The Chon-Kemin event was identified as a reverse faulting event by Molnar and Ghose (2000) because the Chon-Kemin-Chilik fault system was initially interpreted to be a reverse fault system (Chedija, 1986), but other studies have suggested varying amounts of strike-slip movement in addition to the shortening. For example, Kulikova and Krüger (2015) determine a reverse faulting focal mechanism with a minor strike-slip component (264 ± 20° strike, 52 ± 10° dip, and 98 ± 10° rake) from a moment tensor inversion. A significant left-lateral strike-slip component was found by Delvaux et al. (2001) on the Chon-Kemin-Chilik fault segments. Instead, Arrowsmith et al. (2016) find a complex multi-segmented fault rupture consisting of south-dipping segments in the west and north-dipping segments in the central and eastern part of the fault rupture, with a variable dipping angle between 45° and 60°, but with little evidence for strike-slip. In the reference rupture model of the 1911 earthquake, we use the focal mechanism determined by Kulikova and Krüger (2015), i.e. 264 ± 20° strike, 52 ± 10° dip, and 98 ± 10° rake (Table 1).

Although the studies of Arrowsmith et al. (2016) for the 1911 earthquake and Abdrakhmatov et al. (2016) for the 1889 earthquake show evidence of multi-segmented ruptures with step-overs, our rupture models are simplified (Figure 3). Using the mapped fault traces by Arrowsmith et al. (2016) for the 1911 earthquake and Abdrakhmatov et al. (2016) for the 1889 earthquake would not increase the maximum ground shaking in the earthquake scenarios within one standard deviation. The comparison between our rupture model and the potential mapped segments for the 1889 Chilik earthquake shows some differences (Figures 3 and 4). In order to match the observed intensity distribution (Figure 4), our rupture model was extended further NE than the surface ruptures mapped in the field and from satellite

imagery (Abdrakhmatov et al., 2016). Although no surface ruptures have been reported, the NE extension does follow a Quaternary fault scarp. The potential existence of a rupture on the NE scarps means that either the surface effects have been eroded, or the rupture did not reach the earth's surface.

SELECTION OF THE GROUND MOTION MODELS

The choice of an appropriate model for predicting strong ground motion as a function of magnitude and distance is one of the most difficult aspects of seismic hazard studies, regardless of whether they are probabilistic or deterministic, because the hazard estimates are strongly affected by the selected GMPEs, both in terms of expected median prediction and aleatory uncertainty.

It is generally considered good practice in PSHA to try to account for epistemic uncertainty (i.e. the lack of knowledge about which model is best to adopt) by combining different GMPEs in a weighted logic tree (Frankel et al., 2002; Bommer et al., 2005). In contrast, in DSHA a single ground motion model is selected to simulate the earthquake scenario.

We follow the guidance contained in Bommer and Akkar (2010), Stewart et al. (2013) and Stewart et al. (2015) for selecting the most appropriate GMPEs in this study. The Northern Tien Shan is considered an active shallow continental regime (ASCR). We use three GMPEs: Boore and Campbell (2014); Chiou and Youngs (2014); and Akkar et al. (2014). The models of Boore and Atkinson (2014) and Chiou and Youngs (2014) are two GMPEs from the 'Next Generation Attenuation (NGA) - West2' project developed by the Pacific Earthquake Engineering Research Centre in the United States (Bozorgnia et al., 2014; Gregor et al., 2014). This is a large multi-disciplinary program to develop robust GMPEs for crustal earthquakes in ASCR. The NGA-West2 GMPEs were derived from a large database of worldwide strong-motion recordings of earthquakes. The model of Akkar and Bommer

(2013) is derived from a ground motion dataset in Europe and Middle East. The chosen GMPEs are combined in a logic tree and the weights assigned are: 0.35 for Boore et al. (2014), 0.35 for Chiou and Youngs (2014), and 0.30 Akkar et al. (2014).

We consider not only PGA, the most common ground motion parameter in seismic hazard assessment, but also short and longer period spectral accelerations in order to relate the ground shaking to building response. PGA is considered to be a good index to assess the hazard for relatively short buildings (up to 7 stories) (http://earthquake.usgs.gov/hazards/). Longer period accelerations, which may be generated by a large earthquake, attenuate more slowly and are likely to be more significant for taller buildings. For example, a 1.0-s spectral acceleration (SA) may be significant for a 10-story building (e.g. Stein and Wysession, 2003). Long period accelerations may be very important to assess the seismic hazard of Almaty because most of the residential buildings constructed in the last 30 years consist of 4-9 stories (King et al., 2013).

We simulate the earthquake scenario also in terms of intensity, using two intensity prediction equations (IPE): Bindi et al. (2011), as modified by Ullah et al. (2015); and Allen et al. (2012). The IPE of Bindi et al. (2011) was derived from 66 earthquakes in Central Asia with surface wave magnitude between 4.6 and 8.3 and is expressed in terms of MSK-64 scale. The primary distance metric is the epicentral distance and therefore it does not account for the finite extension of the fault rupture. The intensity model of Allen et al. (2012) is derived from a large (> 13000) worldwide dataset of crustal earthquakes of moment magnitude between 5.0 and 7.9 Mw and uses the closest distance to rupture, accounting therefore for the finite dimension of the fault rupture. We assigned a weight of 0.5 to each IPE.

We use rock conditions (i.e. the average shear wave velocity of the top 30 m of material v_{s30}=760 m/s) for the ground motion simulations. This is equivalent to class B in the NEHRP (1994) classification.

HAZARD CALCULATIONS

Using the deterministic approach described in Section "Deterministic approach" and the rupture models in Subsection "Defining the scenario earthquakes", we simulated 1000 ground motion scenarios for each scenario earthquake to account for the uncertainties in the input parameters. Then, we calculated the mean and the standard deviation of the 1000 ground motion values. We found that this number of iterations provides a clear convergence towards constant average and standard deviation without increasing significantly the computational time.

Ground motion scenarios for the 8.0 Mw 1911 Chon-Kemin, 8.2 Mw 1889 Chilik and 7.3 Mw 1887 Verny earthquakes are shown in Figures 5-8, respectively. Figure 5 shows the ground motion scenario of the 1911 Chon-Kemin earthquake on a regular 0.05x0.05° grid covering the area between 42° and 44°N latitude and 74° and 80°E longitude for rock conditions. The strongest ground shaking corresponds to the projection of the fault plane on the surface. The distribution of the 0.2-s SA has the largest values, up to 1.54 ± 0.65 g around the epicentral area (Figure 5). Similar observations can be made for the distribution of the 1889 Chilik earthquake (Figure 6) and the 1887 Verny earthquake (Figure 7). The simulations cover an area of 42° and 45° latitude and 75° and 81° longitude for the 1889 event, and 42° and 45° latitude and 75° and 79° longitude for the 1887 event with a grid resolution of 0.05x0.05° for both events. The distance between Almaty and the epicenter of the earthquakes is 64 km for the 1911 Chon-Kemin earthquake, 146 km for the 1889 Chilik earthquake, and 24 km for the 1887 Verny earthquake. The largest ground motion parameters

475 are recorded for the 1887 earthquake, the closest event to the city, although it has the smallest
476 magnitude.

477 The distribution of the intensity for the three historical earthquakes is shown in Figure 8. The
478 distribution of the standard deviation is uniform within the grid area and is up to I. The
479 intensities in the epicentral area and in Almaty (Figure 8) agree well with the isoseismals in
480 Figure 4. For the 1911 earthquake, we estimated an intensity of IX ± I in the epicentral area
481 and VIII ± I in Almaty; whereas, the isoseismals of Bogdanovich et al. (1914) report an
482 intensity of X in the epicentral area and VIII in Almaty. For the 1889 earthquake, Mushketov
483 (1891) estimate an intensity of IX-X around the Chilik River and VII-VIII in Almaty; and our
484 calculations show an intensity of IX ± I around the epicenter and VIII ± I in Almaty.

485 Table 2 shows the values of PGA and 0.2-s and 1.0-s SA for the three scenario earthquakes
486 for the site in Almaty situated at 43.277°N and 76.896°E. For example, the PGA value for the
487 1911 Chon-Kemin event is 0.230 ± 0.076 g, the 0.2-s SA is 0.48 ± 0.17 g, the 1.0-s SA is
488 0.171 ± 0.069 g, and the MSK-64 intensity is VIII ± I. Clearly, these estimates are associated
489 with large uncertainties and the standard deviations are relatively high, due to the large
490 uncertainty in the GMPE.

491 To check which input parameters has the strongest influence on the earthquake scenarios, we
492 made a sensitivity analysis for Almaty, using the 1911 Chon-Kemin earthquake. We
493 performed eight tests for the sensitivity analysis. In each test, we changed one parameter from
494 the reference rupture model (Table 1) and keep the other parameters constant. The parameters
495 tested include moment magnitude, fault dimensions, soil condition, GMPEs, nodal fault plane
496 orientation, and epicentral location. Table 3 shows the input parameters that were tested in
497 the sensitivity analysis along with the mean and standard deviation of the ground motion
498 values for the site. Most of the tests produce similar results within one standard deviation

(Figure 9). Nevertheless, from the sensitivity analysis we can conclude that the dip angle in the rupture model of the scenario earthquake and the GMPE, together with its aleatory uncertainties, have a strong impact on the deterministic simulations. It is worth analyzing Test 8 that considers a multi-segmented fault rupture. It consists of four segments: from west to east, a 45° south-dipping segment, two 60° north-dipping segments, and a 45° north-dipping segment. The ground motion parameters obtained for Test 8 are smaller than those in the reference model. The reason of this is the following. The fault segment closer to the site has a larger dip angle (dip=60°) in Test 8 than in the reference model (dip=52°), therefore the surface projection of the fault plane is further from Almaty than in the reference model. For this reason, the ground shaking felt in Almaty is smaller. This means that the smaller the dip angle, the largest the ground motion in Almaty because the horizontal projection of the fault plane is closer to the city. For this reason, the largest ground motions are obtained for Test 6 (Figure 9) where the dip angle is 45°.

Probabilistic approach

In this section, we take the results from the previous section and determine the exceedance probabilities for the ground motions of the scenario earthquakes, using PSHA. A probabilistic approach for seismic hazard combines seismological, geological and geophysical data to produce a probabilistic description of the distribution of future shaking that may occur at a site (e.g. Reiter, 1990; McGuire, 2004).

We perform a PSHA using Monte Carlo simulations (e.g. Musson, 1999, 2000, 2012a). Musson (2012a) shows that the Cornell-McGuire PSHA (also referred as to conventional PSHA) and Monte Carlo based PSHA are compatible and provide the same output given the same input.

We construct the source zone model based on the earthquake catalogue (see Appendix), tectonics, geology and kinematic constraints (see Section “Regional setting”) in the Northern Tien Shan. Then, we generate 100,000 synthetic earthquake catalogues, each 100 year long, using Monte Carlo simulations. This can be considered equivalent to a catalogue of 10,000,000 years, which is sufficient to resolve the hazard accurately for long return periods, up to 10,000 years. Each simulated catalogue represents a version of what could occur based on past observed seismicity. The ground motion for the site in Almaty situated at 43.277°N and 76.896°E is computed for each synthetic earthquake. The hazard curve is obtained by counting the number of the results exceeding different probabilities of exceedance (Musson, 2000).

The second stage of the hazard analysis involves disaggregating the hazard results in terms of magnitude, distance and epsilon (ε), i.e. the number of standard deviations above or below the median prediction, to determine whether the scenario earthquakes from our deterministic analysis provide the dominant contribution to the design motion. Using the Monte Carlo simulations, this simply means searching the synthetic catalogues derived from the hazard model for ground motions that are greater than or equal to the design acceleration (plus or minus a small tolerance factor that corresponds to the standard deviation of the design acceleration here) (Musson, 1999).

SEISMIC SOURCE ZONE MODEL

The study area is divided into a series of seismic sources. Seismic activity in each seismic source is considered to be homogeneous in character, and earthquakes have an equal chance of occurring at any point in the zone.

The source model of this work includes the Northern Tien Shan and the South Kazakh Platform because other tectonic structures (e.g. Tarim Basin) are too far (> 400 km distance) from Almaty to be considered relevant to the hazard at the site. The model is based on the seismological, tectonic and geological analysis and consists of 16 zones and two faults (Figure 10). All zones are terminated arbitrarily at the edges of the 400-km radius circle centered in Almaty, as the contribution of earthquakes beyond this radius to the hazard is considered to be negligible.

The faults included in the source models are the Chon-Kemin-Chilik fault system (fault source CKCF) and the Talas-Ferghana fault (fault source TFF). We did not include any other fault systems because the information on their geometry and the maximum magnitude they are capable of generating, is incomplete or unknown. Furthermore, although the overall slip rate of the Tien Shan mountain belt is known (see Section "Regional setting"), it is difficult to distribute it among the active tectonic structures in the region and thus estimate the activity rate of the individual faults. We modelled the Chon-Kemin-Chilik fault system as individual fault in the source model because two of the three scenario earthquakes were generated along it. Its slip rate was estimated using both seismological (e.g. Molnar and Deng, 1984; Molnar and Ghose, 2000) and geodetic data (e.g. Abdrakhmatov et al., 1996; Zubovich et al., 2010); and its geometry is known from the recent geomorphological studies (Delvaux et al., 2001; Arrowsmith et al., 2016; Abdrakhmatov et al., 2016).

The right-lateral strike-slip Talas-Ferghana fault is not well known because no major (Mw > 7.0) earthquakes have occurred along this fault in the last 200 years. Therefore, it is not straightforward to quantify the maximum magnitude it can generate. However, we decided to model it as individual fault in the source model because it is a major tectonic structure in the

567 Norther Tien Shan. Meade and Hager (2001), Zubovich et al. (2007) and Zubovich et al.
568 (2010) estimated an annual slip rate of less than 2 mm/yr. based on geodetic data.

569 **Recurrence statistics**

570 We applied equation (1) to the individual zones of the source model using the catalogue
571 completeness in Appendix and the best regional estimate b = 0.96 as a weighted prior for the
572 zones (see Subsection "Recurrence statistics for the Northern Tien Shan"). The results are
573 shown in Figure 11.

574 The most important sources in the model is the source zone NISK (the North Issyk-Kul
575 region) that contains the three scenario earthquakes used in DSHA (see Section
576 "Deterministic approach"). The best- fit values for equation (1) are N (Mw ≥ 4.5) = 0.90 ±
577 0.13 and b = 0.826 ± 0.078 (Figure 12). This is equivalent to an earthquake somewhere in
578 NISK with a magnitude of 8.0 Mw or above every 864 ± 438 yr. The observed rate for large
579 (Mw ≥ 7.0) earthquakes seldom matches the predicted seismicity by the Gutenberg-Richter
580 law because a 100-year sample of seismicity may contain by chance an earthquake with a
581 recurrence of 1000 years. This is especially true for intraplate areas, such as the Tien Shan,
582 where the earthquake catalogue is shorter (around 138 years) than the potential recurrence
583 interval of the large earthquakes (e.g. Abdrakhmatov et al., 2016; Landgraf et al., 2016). The
584 occurrence of two earthquakes with Mw ≥ 8.0 in 20 years (i.e. the Chilik earthquake in 1889
585 and the Chon-Kemin earthquake in 1911) can be explained by the fact that large intraplate
586 earthquakes cast long shadows in time and their recurrence interval is less regular than the
587 recurrence interval of earthquakes at plate boundaries (e.g. Liu and Stein, 2016). To model
588 the deficit of predicted seismicity for Mw ≥ 7.0 in Figure 12, we treat the seismicity of NISK
589 as two populations of earthquakes: a "normal" activity represented by the predicted

590 seismicity of the Gutenberg-Richter law, and an additional activity consisting of earthquakes
591 in the range 7.0-8.5 Mw. We adopt a similar approach also for the source zone FTS1.

592 We estimated the activity rate of the fault sources from their annual slip rate, using the
593 relationship of Youngs and Coppersmith (1985):

594 $$N(M) = \frac{\mu AS\,(d-b)[1-e-\beta(Mmax-M)]}{bM_o^{max}e^{-\beta(Mmax-M)}} \quad (2)$$

595 Where N is the number of earthquakes above a given magnitude M, S is the annual slip rate,
596 Mmax is the maximum magnitude, M_o^{max} is the seismic moment for Mmax, $A=L*W$ is the
597 area of a W-wide and L-long fault, $\mu=3.3x10^{10}$ N/m^2 is the shear modulus, d is one of the two
598 magnitude-scaling coefficients in the relationship of Kanamori (1977) and Hanks and
599 Kanamori (1979), b is the b-value and $\beta=b*ln(10)$.

600 For the fault source CKCF, we used an annual slip rate between 0.1 and 3 mm/yr. (Thompson
601 et al., 2002) and the b-value of the source zone NISK (i.e. b = 0.826 ± 0.078). We computed
602 an activity rate of N (Mw ≥ 4.5) = 0.14 ± 0.10. This is equivalent to an earthquake with a
603 magnitude of 8.0 Mw or above every 5557 ± 2148 yr.

604 For the fault source TFF, we used a range between 0.1 and 1.5 mm/yr. for the annual slip
605 rate (Zubovich et al., 2010) and the b-value of the entire study area, b = 0.959 ± 0.020 that is
606 similar to the b-value of the neighboring source zones. The activity rate for TFF is N (Mw ≥
607 4.5) = 0.135 ± 0.092 suggesting an earthquake with Mw ≥ 8.0 every 16168 ± 16610 yr.

608 The analysis highlights the difficulty in estimating reliable earthquake rates in regions where
609 the length of seismic record (here around 138 years) is shorter than the average recurrence
610 interval of the largest earthquakes (here at least 864 years for an earthquake of Mw ≥ 8.0).

Other parameters of the source model

Maximum magnitude (Mmax) is the largest possible earthquakes that are considered in the hazard analysis. This is often highly uncertain, though, in a broad sense, the maximum magnitude can be constrained by fault length because any large earthquake requires a sufficiently large structure to host it.

However, this approach cannot be applied in low strain continental interiors, including the Tien Shan, for the following reasons. First, faults in continental interiors are spread over a large region and are usually very segmented (e.g. England and Jackson, 2011). Some of these fault segments are unknown or poorly constrained before an earthquake occurs along them (Campbell et al., 2015; Landgraf et al., 2016; Grutzner et al., 2017). Second, due to the low strain accumulation on the faults, the recurrence interval of large earthquakes is of the order of thousands of years. Therefore, the instrumental and historical records of seismicity probably do not include the largest possible earthquakes (e.g. Abdrakhmatov et al., 2016; Landgraf et al., 2016). This is especially true for the Northern Tien Shan where the earthquake catalogue has a limited length (~138 years). For this reason, it is unconservative not to allow for the possibility of significantly larger events in the future also in zones where the largest historical event is moderate (5-6 Mw). Rather than attempting to assign Mmax on a zone-by-zone basis, the zones were grouped together into larger units where similar tectonic constraints can be applied. The values used for each zone are given in Table 4. Ullah et al. (2015) assign a 8.3 Mmax to the Northern Tien Shan including the Issyk-Kul region (zone NISK) that contains the 8.0 Mw Chon-Kemin earthquake and the 8.2 Mw Chilik earthquake. We think that Mmax=8.3 may be too small in NISK considering the short length of the earthquake catalogue in the Tien Shan and the uncertainty in magnitude (i.e.±0.2). We used

three values of Mmax for NISK (i.e. 8.2, 8.3 and 8.5) with weight of 0.40, 0.40 and 0.20, respectively (Table 4).

The depth distribution of the earthquakes in the Tien Shan and in the South Kazakh Platform is characterized by a distribution between 0 and 40 km (see Subsection "Seismicity in the Northern Tien Shan"). The depth distribution for the model adopted here is shown in Table 5.

The minimum magnitude in the hazard analysis is generally the smallest earthquake considered to be of engineering significance. Here, we assume that the minimum magnitude is 4.5 Mw.

HAZARD CALCULATIONS

Using PSHA and the source model described above, we simulated 100,000 earthquake catalogues, each 100-year long. Each simulation sampled the logic tree of the model according to the branch weights, and the ground motion at the site for each event was estimated using one of the GMPEs in Subsection "Selection of the ground motion models".

The results are expressed as hazard curves that show the annual probability of exceedance as a function of PGA, 0.2-s and 1.0-s SA and MSK-64 intensity for the site in Almaty situated at 43.277°N and 76.896°E (Figure 13). We determined a MSK-64 intensity between VIII and IX and between IX and X for a return period of 475 and 10,000 years, respectively. Ullah et al., 2015) shows a MSK-64 intensity between VII and VIII for a 475 year return period and between IX and X for a 10,000 year return period for Almaty. The comparison with Ullah et al. (2015) is acceptable considering the two studies used different catalogues with different primary magnitude scale (Mw versus M_{LH}), different source models (source model for the Northern Tien Shan versus source model for the entire Central Asia), and different IPEs (Bindi et al., 2011 and Allen et al., 2012 versus Bindi et al., 2011).

The return periods (i.e. the inverse of the annual probability of exceedance) corresponding to the ground motion values simulated for DSHA (see Subsection "Hazard calculations" and Table 2) are obtained by interpolation from the hazard curves in Figure 13 and shown in Table 6. The return periods are associated with large standard deviation because the large variability of the ground motion values propagate into larger uncertainties in the return period. For the MSK-64 intensity the standard deviation of the return period is larger than the return period itself.

In the second stage of the hazard analysis, we disaggregated the hazard results in terms of magnitude, Joyner-Boore distance (Rjb), ε and the originating source zone to determine which earthquake(s) is most likely to produce the hazard values in Table 6. We performed the disaggregation analysis for the design accelerations of the three scenario earthquakes, but we show the results for the 1911 and 1887 earthquakes because they seem to influence more the hazard of Almaty. Disaggregating by zone, we see that the largest influence on the hazard comes from the North Issyk-Kul region (zone NISK) and then the Chon-Kemin-Chilik fault system (fault source CKCF). This is expected because they are next to the site and have high levels of seismicity. Disaggregating the hazard by magnitude, distance and ε, the results are shown in Figures 14 for 0.2 s (i.e. short period acceleration) and Figure 15 for 1.0 s (i.e. long period acceleration). The overall hazard is dominated by earthquakes at close (< 30 km) distances to Almaty. This is explained by the following reason. In the zone NISK, which has a high seismicity, the seismicity is uniformly distributed within the zone and therefore earthquakes have equal chance to occur anywhere in the zone. We modelled explicitly only one fault system, i.e. fault source CKCF, but not other tectonic structures because their geometry, slip rate and maximum magnitude are unknown or not well understood. The disaggregation plot in Figure 14a corresponds to return periods of 122 ± 72 yr. and shows that the hazard is dominated by earthquakes of $4.8 \leq Mw < 5.6$ at distances of less than 10

682 km. Furthermore, the contribution from earthquakes of 7.2 ≤ Mw < 7.6 at distances between
683 20 and 30 km is significant. As the return period increases, the dominant contribution is from
684 large (7.0 ≤ Mw < 8.2) earthquakes (Figure 14b). For long period acceleration and return
685 periods of 152 ± 97 yr., the major contribution to the hazard comes from earthquakes with 7.4
686 ≤ Mw ≥ 7.6 at 20 ≤ Rjb < 30 km (Figure 15a). For return periods of 435 ± 373 yr. and 1-s
687 acceleration, the hazard has strong contribution from earthquakes with 7.4 ≤ Mw < 7.8 at 10
688 ≤ Rjb < 20 km (Figure 15b). For long period acceleration, the contribution to the hazard of
689 Almaty from far distance sources increases, but it is still smaller than that from NISK. The
690 disaggregation analysis for the MSK-64 intensity shows that earthquakes with 7.0 ≤ Mw ≤
691 7.2 at distances between 10 and 20 km influence the hazard (Figure 16).

692 Figures 14-16 clearly suggest that future earthquakes similar to the 1887 Verny earthquake
693 strongly influence the overall seismic hazard of Almaty. However, it is worth underlining that
694 the histograms in Figures 14-16 are very broad due to the uncertainty in the ground motion
695 values computed by the deterministic analysis and used to disaggregate the hazard of Almaty.

696 For a return period of 10,000 years, the ground motion values are: PGA=1.394 g, 0.2-s
697 SA=2.117 g, 1.0-s SA=1.180 g and MSK-64 =X. The disaggregation analysis indicates that
698 the design earthquakes for this return period is given by earthquakes at distances smaller than
699 10 km to Almaty with magnitudes of 7.6 - 7.8 Mw for PGA and the intensity, 7.8 – 8.0 Mw
700 for 0.2-s SA, and 7.4 – 8.0 Mw for 1.0-s SA.

Discussion

The aim of this paper was to gain new insights into the earthquake hazard of the region by using the best available science and combining outcomes from the deterministic and probabilistic approaches in order to reduce the impact of their individual limitations.

First, we applied DSHA for the largest earthquakes occurred in the Northern Tien Shan. Then, we used PSHA to determine the chance of exceeding the deterministic ground motion values and to check whether the scenario earthquakes dominate the hazard of Almaty and therefore should be used as design earthquakes for Almaty. The disaggregation plots show that the design earthquake(s) that dominate the overall seismic hazard for the city is represented by future earthquakes similar to the 1887 Verny earthquake (Figures 14-16). However, these results are associated with large uncertainties due to the large uncertainties in the input parameters propagating into the deterministic ground motion values and the corresponding return periods (Table 6).

The uncertainties in the hazard results reflect the many limitations of our current knowledge on the occurrence of future earthquakes. This is because the hazard results are estimated using incomplete, and sometime misinterpreted data (e.g., earthquake catalogues and fault mapping data) and models (e.g. geodynamic and tectonic models) that are based on a short instrumental earthquake history (a few of hundreds of years in the best case) compared to the geological history (at least some thousands of years) (e.g. Stein et al., 2012). This issue is particularly important in low strain continental environments where the tectonic loading rates are low. For this reason, we cannot say whether the largest earthquakes in the seismic catalogue are also the controlling earthquakes, i.e. the closest and largest potential earthquakes, in the Northern Tien Shan. The great impact of a short earthquake catalogue on

724 the seismic hazard analysis is well underlined in Subsection “Recurrence statistics”. Using
725 the truncated Gutenberg-Richter law we estimated a recurrence intervals between 426 and
726 1302 years for an earthquake of Mw ≥ 8 in the Northern Issyk-Kul region. We think that this
727 estimate seems to under-predict the seismicity for Mw ≥ 7. This explained by the short length
728 of the seismic record (around 138 years) compared to the average recurrence interval of the
729 largest earthquakes (hundreds of years for an earthquake of Mw ≥ 8.0). If we consider the
730 recurrence interval of individual faults, this is even longer, as shown by our recurrence
731 statistics for the Chon-Kemin-Chilik fault system and the Talas-Ferghana fault and confirmed
732 by recent paleoseismological studies (e.g. Campbell et al., 2015; Abdrakhmatov et al., 2016;
733 Landgraf et al., 2016; Grutzner et al., 2017). For example, Abdrakhmatov et al. (2016) find
734 evidences that the fresh scarp on the Saty fault segment associated with the 1889 Chilik
735 earthquake was the only surface-rupturing event in the last 5000 years. Landgraf et al. (2016)
736 find evidences of paleoearthquakes on a fault situated in the Kyrgyz ranges of the Tien Shan,
737 near Bishkek (Kyrgyzstan) and infer a recurrence interval of several thousand years for a
738 large earthquake on that fault. Moreover, the concept of regular recurrence interval may not
739 be applicable to intraplate continental regions where faults are widespread, highly segmented
740 and often poorly mapped, and the tectonic loading of the faults is slow and variable due to the
741 interaction between faults (e.g. Liu and Stein, 2016).

742 Although our rupture model of the scenario earthquakes may be considered simplified, it
743 provides a good representation of the potential ground motion that might be produced by
744 future earthquakes and that is similar to those that occurred in the past within the standard
745 deviation of the input parameters (e.g. rupture geometry, location and magnitude). This was
746 possible by combining seismological data and geological observations and allows us to
747 overcome some of the limitations in each type of data. For example, the short length of
748 seismic record and the inherent uncertainty in the location and magnitude of earthquakes can

749 be limited by mapping active faults and characterizing the fault source using paleoseismology
750 and geomorphology and geodetics. Similarly, the observations from paleoseismology,
751 geomorphology can be checked against our current understanding of earthquake physics and
752 the existing worldwide and regional earthquake catalogue to ensure their consistency. An
753 example of this is given in Subsection "Defining the scenario earthquakes" where we
754 combined findings from recent geomorphological and paleoseismological studies with
755 equations used in earthquake physics (e.g. empirical magnitude scaling relationships and the
756 definition of M_0 and Mw).

757 Using both PSHA and DSHA is recommended for the seismic hazard of highly critical
758 infrastructures, such as dams (ICOLD, 2010) and nuclear power plants (IEAE, 2010). The
759 standard practice is to perform PSHA and then to apply DSHA for the worst-case scenario.
760 Integrating the outcomes from DSHA and PSHA may be also a powerful tool for community-
761 based risk activity and earthquake reduction management. The development of simple
762 deterministic scenarios for potential future earthquakes, together with their probabilistic
763 dimension, would contribute to translate the effects of earthquakes into real-life impact (ODI,
764 2016). This is especially important in densely populated areas in continental low strain rate
765 environments, such as Almaty, where the largest recorded earthquakes occurred in historical
766 or prehistorical time and therefore collective memory of those disasters in the population and
767 society reduces with time.

768 Conclusions

769 This work has highlighted the importance of integrating the outcomes from PSHA and DSHA
770 to reduce, and possibly overcome, the current limitations in seismic hazard analysis and
771 seismological, geological and geodetic data.

772 The main finding of the paper is that the major contribution to the seismic hazard of Almaty
773 comes from earthquakes with 7.0 ≤ Mw ≤ 7.8 close (< 30 km) to Almaty at return periods
774 smaller than 1000 years. Future earthquakes similar to the 7.3 Mw 1887 Verny earthquake
775 dominate the overall hazard of Almaty. However, these estimates are associated with large
776 uncertainties. Therefore, future research should focus in reducing the uncertainties in the
777 rupture model by mapping the faults in the region, especially around Almaty, searching for
778 evidence of the occurrence of paleo-earthquakes on them and characterizing the source of the
779 Verny earthquake that is the least well constrained of the three destructive historical
780 earthquakes recorded in the Northern Tien Shan between the end of the 19th and the
781 beginning of the 20th century. The assessment of the seismic hazard for Almaty should also
782 include the effects of local site geology that may results in de-amplifying or amplifying the
783 ground motions. These may have a strong impact in regions where the cities are situated in
784 valleys and depressions, such as Almaty (Pilz et al., 2015). Any new information should then
785 be used to update the seismic hazard for Almaty.

786 Data and Resources

787 The online database of the International Seismological Centre is at http://www.isc.ac.uk (last
788 accessed November 2016). All the other data used in this paper came from published sources
789 listed in the references. The plots were made using the Generic Mapping Tools version 4.5.2
790 (www.soest.hawaii.edu/gmt; Wessel and Smith, 2013).

Acknowledgements

This work was funded by the Natural Environmental Research Council under the grant Earthquake without Frontiers EwF_NE/J02001X/1_1.

Appendix

The earthquake catalogue of this work contains data from three sources. The International Seismological Centre (ISC) Bulletin is generally regarded as a definitive record of the Earth's instrumental seismicity and contains data from 1900 to the present. The World Seismicity Database (WSD) of the British Geological Survey (Henni et al., 1998) contains parametric data for earthquakes from 2500 BC onwards and has been compiled over a period of thirty years from various catalogues. The earthquake catalogue for the "Earthquake Model for Central Asia" (EMCA) project (Mikhailova et al., 2015) includes information for 33620 earthquakes that occurred in Central Asia in the period from 2000 BC to 2009 AD, although most of the entries (i.e. 33378) are for earthquakes that occurred after 1900.

It is standard practice in seismic hazard assessment to use moment magnitude Mw (Bolt and Abrahamson, 2003). However, the earthquake data contain magnitude estimates in different magnitude scales. Therefore, we convert the magnitude estimates to Mw using the equations of Scordilis (2006), which are based on a large global dataset of earthquakes and comprises various tectonic regimes.

For example, the ISC catalogue contains a number of different magnitude estimates for each earthquake determined by different agencies that reported the event (e.g. surface-wave magnitude Ms, body-wave magnitude mb, Mw). We used the hierarchy in Table 7 to select

812 one magnitude from the available estimates. Similarly, we apply a hierarchical approach to
813 the WSD data because they also contain different magnitude estimates determined by
814 different agencies.

815 The EMCA catalogue merges many sources and magnitude scales. The magnitude of this
816 catalogue is the surface wave magnitude according to the Moscow-Prague formula (Karnik,
817 1962) and indicated as M_{LH} in the Russian scientific literature. The original magnitude of the
818 earthquakes is not indicated (Mikhailova et al., 2015; Ullah et al., 2015). We used only events
819 with $M_{LH} \geq 5.4$ from the EMCA catalogue if they were not included in the ISC and WSD
820 database. The reason is that the uncertainty in the magnitude conversion $M_{original} \rightarrow M_{LH} \rightarrow Mw$
821 becomes large for $M_{LH} < 5.4$ and may produce an overestimation in the final Mw value
822 (Scordilis, 2006).

823 **DECLUSTERING AND COMPLETENESS**

824 To decluster the earthquake catalogue and therefore remove the dependent events
825 (aftershocks and foreshocks) from the catalogue, we use the approach of Musson (1999,
826 2000), which is a modified version of the moving window method of Reasenberg (1985).
827 Analysis of the catalogue shows that the most appropriate window in time and space has a
828 length of 30 days and 30 km, respectively. If an earthquake is identified as a mainshock, all
829 events within 30 km of the epicentre and 30 days before and after that event are considered to
830 be dependent events.

831 To assess the completeness of the catalogue as a function of time, we use the statistical
832 approach of Stepp (1972), modified by Musson (2000), to assess the earthquake catalogue
833 completeness. This is based on the estimators of the mean seismicity rate of earthquakes for
834 different magnitude ranges and time windows. Our analysis suggests that the catalogue is

835 complete for moderate (> 4.5 Mw) magnitudes for the second half of the twentieth century
836 (Table 8). This estimate corresponds to the deployment of the World-Wide Standardardized
837 Seismographic Network in the early 1960s. The historical record of seismicity in the Tien
838 Shan is relatively short and, even for large (Mw ≥ 7) events, is probably complete only since
839 the 1880s when the construction of Russian fortresses started in the region (Molnar and
840 Deng, 1984; Korjenkov et al., 2003). The magnitude thresholds in Table 8 agree with the
841 completeness analysis of the EMCA earthquake catalogue for Mw ≥ 5.5, but our
842 completeness analysis is more conservative for smaller magnitudes.

843 References

844 Abdrakhmatov, K., S. A. Aldazhanov, B. H. Hager, M. W. Hamburger, T. A. Herring, P. Molnar, S.
845 V. Panasyuk, M. T. Prilepin, R. Reilinger, I. S. Sadybakasov, B. J. Souter, Y. A. Tapeznikov, V. Y.
846 Tsurkov, and A. V. Zubovich (1996). Relatively recent construction of the Tien Shan inferred from
847 GPS measurements of present-day crustal deformation rates. *Nature* **384** 450-453.
848
849 Abdrakhmatov, K., K. Djanuzakov, and D. Delvaux (2002). Active tectonics and seismic hazard of
850 the Issyk-Kul basin in the Kyrgyz Tian Shan, in *Lake Issyk-Kul: Its natural environment*. Klerkx, J.,
851 and B. Imanackunov (Editors), Kluwer Academic Publishers, Dordrecht, 147-160.
852
853 Abdrakhmatov, K., R. Walker, G. Campbell, A. Carr, A. Elliott, C. Hillmann, J. Hollingsworth, A.
854 Landgraf, D. Mackenzie, A. Mukambayev, M. Rizza, and R. R. Sloan (2016). Multi-segment rupture
855 in the July 11th 1889 Chilik earthquake (Mw 8.0-8.3), Kazakh Tien Shan, identified from remote-
856 sensing, field survey, and paleoseismic trenching. *J. Geophys. Res.* **121** 4615-4640.

857

Abe, K., and S. Noguchi (1983). Determination of magnitude for large shallow earthquakes 1898-1917. *Phys. Earth Planet. In.* **32** 45-59.

Abrahamson, N. A. (2000). State of the practice of seismic hazard evaluation, *Proc. Geo Eng., 19-24 November 2000, Melbourne, 659-685*.

Abrahamson, N. A. (2006). Seismic hazard assessment: Problems with current practice and future developments, in *Proceedings of the First European Conference on Earthquake Engineering and Seismology*, Geneva, Switzerland, Keynote Address K2.

Aki, K. (1966). Generation and propagation of G waves from the Niigata earthquake of June 16, 1964: Part I. A statistical analysis, *Bull. Earthquake Res. Inst.* **44** 23-72.

Akkar, S., M.A. Sandikkaya and J. J. Bommer (2014). Empirical ground motion models for point- and extended-source crustal earthquake scenariosin Europe and the Middle East, *Bull. Earthquake Eng.* **12** 359-387.

Alinaghi, A., and F. Krüger (2014). Seismic array analysis and redetermination of depths of earthquakes in Tien-Shan: implications for strengths of the crust and lithosphere, *Geophys. J. Int.* **198** 1111-1129.

Allen, T.I., D.J. Wald, and C.B. Worden (2012). Intensity attenuation for active crustal regions, *J.Seismol.* **16** 409-433.

Amante, C. and B. Eakins (2009). ETOPO1 1Arc-Minute Global Relief Model: Procedures, data resources and analysis, *Technical Memorandum NESDIS NGDC-24*, National Geophysical Data Center, NOAA, doi:10.7289/V7285C8276M.

886 Arrowsmith, J., C. Crosby, A. Korjenkov, E. Mamyrov, I. Povolotskaya, B. Guralnik, and A.
887 Landgraf (2016). Surface rupture of the 1911 Kemin (Chon-Kemin) earthquake, Northern Tien Shan,
888 Kyrgyzstan, *Geol. Soc. Spec. Publ.* ***432*** doi:10.1144/SP432.10.
889
890 Aspinall, W.P. (2013). Scientific uncertainties: a perspective from probabilistic seismic hazard
891 assessments for low-seismicity areas, in *Risk and Uncertainty Assessment for Natural Hazards*.
892 Rougier, J., S. Sparks, and H. L. Jill (Editors), Cambridge University Press, Cambridge, 234-274.
893
894 Besstrashnov, V. (1993). Report on the results of seismo-geological ínvestigations in the area of the
895 Mainak Water-Power Plant on the Charyn River. Hydroproject Association, Unpublished Report (in
896 Russian).
897
898 Bindi, D., S. Parolai, A. Oth, K. Abdrakhmatov, A. Muraliev, and J. Zchau (2011). Intensity
899 prediction equations for Central Asia, *Geophys. J. Int.* **187** 327-337.
900
901 Bindi, D., S. Parolai, A. Gmez-Capera, M. Locati, Z. Kalmetyeva, and N. Mikhailova (2014).
902 Locations and magnitudes of earthquakes in Central Asia from seismic intensity data, *Journal of*
903 *Seismology* **18** 1-21.
904
905 Bogdanovich, K., I. Kark, B. Korol'Kov, and D. Mushketov (1914). Earthquake in Northern district
906 of Tien-Shan, 22 December 1910 (4 January 1911), *Commission of the Geology Committee,* St.
907 Petersburg, Russia.
908
909 Bolt, B. A., and N. A. Abrahamson (2003). Estimation of strong seismic ground motions, in
910 *International Handbook of Earthquake and Engineering Seismology*. Lee, W. H. K., H. Kanamori, P.
911 C. Jennings, and C. Kisslinger (Editors), Academic Press, San Diego, 983-1001.
912

913 Bommer, J. J., F. Scherbaum, H. Bungum, F. Cotton, F. Sabetta, and N. A. Abrahamson (2005). On
914 the use of logic trees for ground-motion prediction equations in seismic-hazard analysis, *Bull.*
915 *Seismol. Soc. Am.* **95** 377-389.
916
917 Bommer, J. J. and S. Akkar (2010). On the selection of ground-motion prediction equations for
918 seismic hazard analysis, *Seismol. Res. Lett.* **81** 783-793.
919
920 Boore, D., J. Stewart, E. Seyhan, and G. Atkinson (2014). NGA-West2 equations for predicting PGA,
921 PGV, and 5% damped PSA for shallow crustal earthquakes, *Earthquake Spectra* **30** 1057-1085.
922
923 Bozorgnia, Y., N.A. Abrahamson, L. Al Atik, T.D. Ancheta, G.M. Atkinson, J.W. Baker, A. Baltay,
924 D.M. Boore, K.W. Campbell, B. Chiou, R. Darragh, S. Day, J. Donahue, J., R.W. Graves, N. Gregor,
925 T. Hanks, I.M. Idriss, R. Kamai, T. Kishida, A. Kottke, S.A. Mahin, S. Rezaeian, B. Rowshandel, E.
926 Seyhan, S. Shai, T. Shantz, W. Silva, P. Spudich, J.P. Stewart, J. Watson-Lamprey, K. Wooddell, and
927 R. Youngs (2014). NGA-West2 research project, Earthquake Spectra 30, 973–987.
928
929 Bullen, M. E., D. W. Burbank, J. J. Garver, and K. Abdrakhmatov (2001). Late Cenozoic tectonic
930 evolution of the north-western Tien Shan: new age estimates for the initiation of mountain building,
931 *Bull. Geol. Soc. Am.* **113** 1544-1559.
932
933 Burtman, V.S., S.F. Skobelev, and P. Molnar (1996). Late Cenozoic slip on the Talas-Ferghana fault,
934 the Tien Shan, central Asia, *Bull. Seismol. Soc. Am.* **108** 1004-1021.
935
936 Buslov, M. M., J. Klerkx, K. Abdrakhmatov, D. Delvaux, V. Y. Batalev, O. A. Kuchai, B.
937 Dehandschutter, and A. Muraliev (2003). Recent strike-slip deformation of the northern Tien Shan,
938 *Geol. Soc. Spec. Publ.* **210** 53-64.
939

940 Campbell, G., R. Walker, K. Abdrakhmatov, J.-L. Schwenninger, J. Jackson, J. Elliott, and A. Copley
941 (2013). The Dzhungarian fault: Late Quaternary tectonics and slip rate of a major right-lateral strike-
942 slip faulting the northern Tien Shan region, *J. Geophys. Res.***118** 5681-5698.
943
944 Campbell, G., R. Walker, K. Abdrakhmatov, J. Jackson, J. Elliott, D. Mackenzie, T. Middleton, and
945 J.-L. Schwenninger (2015). Great earthquakes in low strain rate continental interiors: An example
946 from SE Kazakhstan, *J. Geophys. Res.***120** 5507-5534.
947
948 Castellaro, S., F. Mulargia, and Y.Y. Kagan (2006). Regression problems for magnitudes, *Geophys. J.*
949 *Int.*, **165** 913-930.
950
951 Chedija, O. (1986). *Morpho-structures and recent tectonism in the Tien Shan* (in Russian), Ilim,
952 Frunze.
953
954 Chiou, B., and R. R. Youngs (2014). Update of the Chiou and Youngs NGA model for the
955 average horizontal component of peak ground motion and response spectra, *Earthquake Spectra* **30**
956 1117-1153.
957
958 Crosby, C., J. Arrowsmith, A. Korjenkov, B. Guralnik, E. Mamyrov, and I. Povolotskaya (2007). The
959 hunt for the surface rupture from the 1889 Ms 8.3 Chilik earthquake, Northern Tien-Shan, Kyrgyzstan
960 and Kazakhstan, *AGU Fall Meeting Abstract*, F5, Poster Presentation.
961
962 Delvaux, D., K. Abdrakhmatov, and A. Strom (2001). Landslide and surface breaks of the 1911 M 8.2
963 Kemin earthquake, *Landslides* **42** 1583-1592.
964
965 De Mets, C., R. G. Gordon, D. F. Argus, and S. Stein (1990). Current plate motions, *Geophys. J. Int.*
966 **101** 425-478.
967

968 England, P., and J. Jackson (2011). Uncharted seismic risk, *Nature Geoscience* **4** 348-349.
969
970 Frankel, A.D., M. D. Petersen, C. S. Mueller, K. M. Haller, R. L. Wheeler, E. V. Leyandecker, R. L.
971 Wesson, S. C. Harmsen, C. H. Cramer, D. M. Perkins, K. S. Rukstales (2002). Documentation for the
972 2002 update of the national seismic hazard maps, *U.S. Geological Survey Open-file report 02-420*.
973
974 Ghose, S., R. J. Mellors, A. Korjenkov, M. W. Hamburger, T. L. Pavlis, G. L. Pavlis, M. Omuraliev,
975 E. Mamyrov, and A. Mraliev (1997). The Ms = 7.3 1992 Suusamyr, Kyrgyzstan, earthquake in the
976 Tien Shan: 2. Aftershock focal mechanisms and surface deformation, *Bull. Seismol. Soc. Am.* **87** 23-
977 28.
978
979 Gregor, N., N.A. Abrahamson, G. M. Atkinson, D. M. Boore, Y. Bozorgnia, K. W. Campbell, B.
980 Chiou, I. M. Idriss, R. Kamai, E. Seyhan, W. J. Silva, J. Stewart, and R. R. Youngs (2014).
981 Comparisons of the NGA-West2 GMPEs, *Earthquake Spectra* **30(3)** 1179-1197.
982
983 Grützner, C., E. Carson, R.T. Walker, E. J. Rhodes, A. Makambayev, D. Mackenzie, J. R. Elliott,
984 G.E. Campbell, and K. Abdrakhmatov (2017). Assessing the activity of faults in continental interiors:
985 Paleoseismic insights from SE Kazakhstan, *Earth Planet. Sci. Lett.* **459** 93-104.
986
987 Gupta, I. (2002). The state of the art in seismic hazard analysis, *ISET J. Earthquake Tech.* **39** 311-346.
988
989 Gutenberg, B., and C. F. Richter (1954). *Seismicity of the Earth and associated phenomena*, Princeton
990 University Press.
991
992 Hanks, T., and H. Kanamori (1979). A moment magnitude scale, *J. Geol. Res.* **84** 2348-2350.
993
994 Henni, P. H. O., C. J. Fyfe, and P. C. Marrow (1998). The BGS World Seismicity Database, *Technical*
995 *Report WL/98/13*.

IAEA - International Atomic Energy Agency (2010). Seismic hazards in site evaluation for nuclear installations. *Specific Safety Guide No. SSG-9, IAEA, Vienna*.

ICOLD (2010). Selecting seismic parameters for large dams. *ICOLD Committee, Bulletin 72*.

Johnston, A.C., K. J. Coppersmith, L. R. Kanter, and C. A. Cornell (1994). The earthquakes of stable continental regions, *EPRI Report*, Electric Power Research Institute, Palo Alto.

Kanamori, H. (1977). The energy release in great earthquakes, *J. Geophys. Res.* **82** 2981-2987.

Karnik, V. (1962). Amplitude-distance curves of surface waves at short epicentral distances, *Stud. Geophys. Geod.* **6** 340-346.

King, S.A., V.I. Khalturin, and B.E. Tucker (2013). *Seismic hazard and building vulnerability in Post-Soviet Central Asian Republics*, Springer, Berlin.

Klügel, J.-U. (2005). Problems in the application of the SSHAC probability method for assessing earthquake hazards at Swiss nuclear power plants, *Eng. Geo.* **78** 285-307.

Klügel, J.-U. (2008). Seismic Hazard Analysis - Quo vadis?, *Earth-Sci. Rev.* **88** 1-32.

Kondorskaia, N., N. Shebalin, and World Data Center for Solid Earth Geophysics (1982). *New catalogue of strong earthquakes in the USSR from ancient times through 1977*. Report.

Kondorskaya, N., and N. Shebalin (1977). *New catalogue of large earthquakes in the USSR area*, Nauka.

1024 Kondorskaya, N., and N. Shebalin (1982). *New catalogue of strong earthquakes in the USSR from*
1025 *ancient times through 1977*, National Oceanic and Atmospheric Administration, Boulder, Colorado.
1026
1027 Korjenkov, A., K. Baipakov, C. Chang, Y. Peshkov, and T. Savelieva (2003). Traces of ancient
1028 earthquakes in Medieval cites along the Silk Road, northern Tien Shan and Dzhungaria, *Turk. J. Earth*
1029 *Sci*. **12** 241-261.
1030
1031 Kramer, S. (1996). *Geotechnical Earthquake Engineering*, Prentice Hall, New Jersey.
1032
1033 Krinitzsky, E. L. (2003). How to combine deterministic and probabilistic methods for assessing
1034 earthquake hazards, *Eng. Geol.* **70** 157-163.
1035
1036 Krüger, F., A. Kulikova, and A. Landgraf (2016). Instrumental magnitude constraints for the 11 July
1037 1889, Chilik earthquake, *Geol. Soc. Spec. Publ.* **432** doi:10.1144/SP432.8.
1038
1039 Kulikova, G., and F. Krüger (2015). Source process of the 1911 M8.0 Chon-Kemin earthquake:
1040 investigation results by analogue seismic records, *Geophys. J. Int.* **201** 1891-1911.
1041
1042 Landgraf, A., A. Dzhumabaeva, K. Abdrakhmatov, M.R. Stecker, E.A. Macaulay, J. Arrowsmith, H.
1043 Sudhaus, F. Preusser, G. Rugel, and S. Merchel (2016). Repeated large-magnitude earthquakes in a
1044 tectonically active, low-strain continental interior: The Northern Tien Shan, Kyrgyzstan, *J. Geophys.*
1045 *Res. Solid Earth Planets* **121** 3888-3910.
1046
1047 Leonard, M. (2010). Earthquake fault scaling: Self-consistent relating of rupture length, width,
1048 average displacement, and moment release, *Bull. Seismol. Soc. Am.* **100** 1971-1988.
1049
1050 McGuire, R. K. (2001). Deterministic vs. probabilistic earthquake hazards and risks, *Soil Dynam.*
1051 *Earthquake Eng.* **21** 377-384.

McGuire, R. K. (2004). *Seismic Hazard and Risk Analysis,* Earthquake Engineering Research Institute, Oakland.

Meade, B. J., and B. H. Hager (2001). The current distribution of deformation in the western Tien Shan from block models constrained by geodetic data, *Geol. Geofiz.* **42** 1622–1633

Mellors, R.J., F.L. Vernon, G.L. Pavlis, G.A. Abers, M.W. Hamburger, S. Ghose, and B. Iliasov (1997). The Ms=7.3 1992 Suusamyr, Kyrgyzstan, earthquake: 1. Constraints on fault geometry and source parameters based on aftershocks and body-wave modelling, *Bull. Seismol. Soc. Am.* **87** 11-22.

Mikhailova, N., A. Mukambayev, I. Aristova, G. Kulikova, S. Ullah, M. Pilz, and D. Bindi (2015). Central Asia earthquake catalogue from ancient time to 2009, *Ann. Geophys.* **58** doi:10.4401/ag-6681.

Molnar, P., and Q. Deng (1984). Faulting associated with large earthquakes and the average rate of deformation in central and eastern Asia, *J. Geophys. Res.* **89** 6203-6228.

Molnar, P., and S. Ghose (2000). Seismic moments of major earthquakes and rate of shortening across the Tien Shan, *Geophys. Res. Lett.* **27** 2377-2380.

Mushketov, I. (1890). The Verny earthquake 28th May (9th June) 1887. *Memoirs of the Geological Committee* **10(1)** St. Petersburg.

Mushketov, I. (1891). Materials for investigation of earthquakes in Russia. *Annex to the 27th volume of tidings of the Imperial Russian Geographical Society*.

Musson, R. M. W. (1999). Determination of design earthquakes in seismic hazard analysis through Monte Carlo simulation, *J. Earthquake Eng.* **3** 463-474.

Musson, R. M. W. (2000). The use of Monte Carlo simulations for seismic hazard assessment in the UK, *Ann. Geophys.* **43** 1-9.

Musson, R. M. W. (2012a). PSHA Validated by Quasi Observational Means, *Seismol. Res. Lett.* **83** 130-134.

Musson, R.M.W. (2012b). The effect of magnitude uncertainty on activity rates, *Bull. Seismol Soc. Am.* **102** 2771-2775.

NEHRP (1994). Recommended provisions for seismic regulations for new buildings and other structures, Part 1: Provisions, *FEMA 222A Building Seismic Safety Council*, Washington D.C.

ODI – Overseas Development Institute (2016). Earthquake science and hazard in Central Asia. *Conference Summary Report.*

Paul, J., R. Burgmann, V.K. Gaur, R. Bilham, K. Larson, M.B. Ananda, S. Jade, M. Mukal, T.S. Anupuma, G. Satyal, and D. Kumar (2001). The motion and active deformation of India, *Geophys. Res. Lett.* **28** 647-650.

Pilz, M., T. Abakanov, K. Abdrakhmatov, D. Bindi, T. Boxberger, B. Moldobekov, S. Orunbaev, N. Sylacheva, S. Ullah, S. Usupaev, P. Yasunov, and S. Parolai (2015). An overview on the seismic microzonation and site effect studies in Central Asia, *Ann. Geophys*. **58** doi: 10.4401/ag-6662.

Reasenberg, P. A. (1985). Second-order moment of Central California seismicity, 1969-1982, *J. Geophys. Res.* **90** 5479-5495.

Reigber, C., G. Michel, R. Galas, D. Angermann, J. Chen, A. Papschev, R. Arslanov, V. Tzurkov, and M. Ishanov (2001). New space geodetic constraints on the distribution of deformation in Central Asia, *Earth Planet. Sci. Lett.* **191** 157-165.

Reiter, L. (1990). *Earthquake Hazard Analysis: Issues and Insights*, Columbia University Press, New York.

Rhoades, D.A. (1996). Estimation of the Gutenberg-Richter relation allowing for individual earthquake magnitude uncertainties. *Tectonophysics* **258** 71-83.

Rhoades, D.A. and D. J. Dowrick (2000). Effects of magnitude uncertainties on seismic hazard estimates, *Proc.12th World Conf. Earthquake Eng*., Wellington, New Zealand, Paper 1179.

Scordilis, E. M. (2006). Empirical global relations converting Ms and mb to moment magnitude, *Journal of Seismology* **10** 225-236.

Sloan, R.A., J. Jackson, D. McKenzie, and K. Priestley (2011). Earthquake depth distribution in Central Asia, and their relations with lithosphere thickness, shortening, and extension, *Geophys. J. Int.* **185** 1-29.

Stepp, J. C. (1972). Analysis of completeness of the earthquake sample in the Puget sound area and its effect on statistical estimates of earthquake hazard, *First International Conference on Microzonation*, Seattle, **2** 897-909.

Stein, S., and M. Wysession (2003). *An Introduction to Seismology, Earthquakes, and Earth Structure*, Wiley-Blackwell Publishing, Oxford.

1134 Stein, S., and M. Liu (2016). Mid-continent earthquakes: Spatiotemporal occurrences, causes and
1135 hazards. *Earth-Sci. Rev.* **162** 364-386.
1136
1137 Stein, S, R. J. Geller, and M. Liu (2012). Why earthquake hazard maps often fail and what to do about
1138 it, *Tectonophysics*, **562-563** 1-25.
1139
1140 Stewart, J., J. Douglas, M. Javanbarg, C. Di Alessandro, Y. Bozorgnia, N. A. Abrahamson, D. Boore,
1141 K. Campbell, E. Delavaud, M. Erdik, P. J. Stafford (2013). GEM-PEER Task 3 Project: Selection of a
1142 Global Set of Ground Motion Prediction Equations, *PEER Report 2013/22.*
1143
1144 Stewart, J., J. Douglas, M. Javanbarg, Y. Bozorgnia, N. A. Abrahamson, D. Boore, K. Campbell, E.
1145 Delavaud, M. Erdik, P. J. Stafford, P., 2015. Selection of Ground Motion Prediction Equations for the
1146 Global Earthquake Model, *Earthquake Spectra* **31** 19-45.
1147
1148 Stock, C., and E.G.C. Smith (2000). Evidence for different scaling of earthquake source parameters
1149 for large earthquakes depending on faulting mechanism, *Geophys. J. Int.* **143** 157-162.
1150
1151 Storchak, D., D. Di Giacomo, I. Bondár, E. Engdhal, J. Harris, W. Lee, A. Villasenor, and P.
1152 Bormann (2013). Public release of the ISC-GEM global instrumental earthquake catalogue (1900-
1153 2009), *Seismol. Res. Lett.* **84** 810-815.
1154
1155 Tapponnier, P., and P. Molnar (1979). Active faulting and Cenozoic tectonics of the Tien Shan,
1156 Mongolia and Baykal regions, *J. Geophys. Res.* **84** 3425-3456.
1157
1158 Tatevossian, R.E. (2007). The Verny, 1887, earthquake in Central Asia: Application of the INQUA
1159 scale, based on coseismic environmental effects, *Quatern. Int.* **173** 23-29.
1160

1161 Thompson, S. C., R. J. Weldon, C. M. Rubin, and K. Abdrakhmatov (2002). Late Quaternary slip
1162 rates across the central Tien Shan, Kyrgyzstan, Central Asia, *J. Geophys. Res.* **107**
1163 doi:10.1029/2991JB000596.
1164
1165 Tibaldi, A., E. Graziotto, F. Forcella, and V. Gapich (1997). Morphotectonic indicators of Holocene
1166 faulting in central Tien Shan, Kazakhstan, and geodynamic implications, *J. Geodyn*. **23** 23-45.
1167
1168 Tinti, S., and F. Mulargia (1985). Effects of magnitude uncertainties on estimating the parameters in
1169 the Gutenberg-Richter frequency-magnitude law, *Bull. Seismol. Soc. Am.* **75** 1681-1697.
1170
1171 Ullah, S., D. Bindi, M. Pilz, L. Danciu, G. Weatherill, E. Zuccolo, A. Ischuk, N. Mikhailova, K.
1172 Abdrakhmatov, and S. Parolai (2015). Probabilistic seismic hazard assessment for Central Asia, *Ann.*
1173 *Geophys*. **58** doi:10.4401/ag-6687.
1174
1175 Youngs, R.R., and K.J. Coppersmith (1985). Implications of fault slip rates and earthquake
1176 recurrence models to probabilistic seismic hazard estimates. *Bull. Seismol. Soc. Am.*
1177 **75 (4)** 939-964.
1178
1179 Wang, Z., and J. Cobb (2012). A critique of probabilistic versus deterministic seismic hazard analysis
1180 with special reference to the New Madrid seismic zone, in *Recent advances in North American*
1181 *Paleoseismology and Neotectonics East of the Rockies* Cox, R. T., M. P. Tuttle, and O. S. Boyd
1182 (Editors), *Geol. Soc. Am. Spec. Publ.* **493** 259-275.
1183
1184 Wessel, P., W. Smith, R. Scharroo, J. Luis, and F. Wobbe (2013). Generic Mapping Tools: Improved
1185 version released, *EOS, Trans. AGU.* **94** 409-410.
1186

Zöller, G., S. Ullah, D. Bindi, S. Parolai, and N.N. Mikhailova (2017). The largest expected earthquake magnitudes in Central Asia: statistical inference from an earthquake catalogue with uncertain magnitudes. *Geol. Soc. Spec. Publ.* ***432*** 29-32.

Zubovich, A. V., V. I. Makarov, S. I. Kuzikov, O. I. Mosienko, and G. G. Shchelochkov (2007). Intracontinental mountain building in central Asia as inferred from satellite geodetic data (in Russian), *Geotektonika* **41** 16–29.

Zubovich, A., X. Wang, Y. Scherba, G. Schelochkov, R. Reilinger, C. Reigber, O. Mosienko, P. Molnar, W. Michajilow, W. Makarov, J. Li, S. Kuzikov, T. Herring, M. Hamberger, B. Hager, Y. Dang, V. Bragin, and R. Beisenbaev (2010). GPS velocity field for the Tien Shan and surrounding regions, *Tectonics* **29** doi:10.1029/2010TC002772.

List of figure captions

Figure 1: (a) Topographic map of Asia from the global model ETOPO1 (Amante and Eakins, 2009). The white line represents the plate boundaries and the dashed rectangle indicates the study area. (b) Seismo-tectonic map of the Northern Tien Shan mountain belt where historical (before 1964) seismicity is indicated by squares and instrumental (after 1964) seismicity, by circles. Symbol size is proportional to magnitude. Events of unknown depth are colored white. Tectonic structures are from: 1) the Kyrgyz Institute of Seismology and digitized by the Active Tectonics Group at Arizona State University; 2) Hager et al. at Central Washington University; and Bogdanovich et al. (1914) and digitized by the Active Tectonics Group at Arizona State University. CKCF and TFF stand for Chon-Kemin-Chilik fault and

Talas-Ferghana fault, respectively. The Ferghana Basin and Lake Issyk-Kul are indicated by FB and LIK, respectively.

Figure 2: Magnitude-frequency recurrence for the study area.

Figure 3: Location of the epicenters and fault ruptures of the three scenario earthquakes in this study. The dashed lines indicate the fault segments mapped by Abdrakhmatov et al. (2016) that potentially ruptured during the 1889 Chilik earthquake. The dotted lines indicate the surface rupture mapped by Arrowsmith et al. (2016) for the 1911 Chon-Kemin earthquake. See Figure 1 for details on the tectonic structures.

Figure 4: Isoseismals for the 1911 Chon-Kemin (Bogdanovich et al., 1914) and 1889 Chilik (Mushketov et al., 1891) earthquakes are indicated in black and grey, respectively. The star represents Almaty. Locations of the epicenter and fault rupture of the two earthquakes are also indicated.

Figure 5: Distribution of PGA and 0.2-s and 1.0-s SA, together with their standard deviation, for the 1911 Chon-Kemin earthquake. The mean ground motions and their standard deviations have been computed from 1000 scenarios. The white star indicates the city of Almaty. The white dot and the white line describe the epicenter and the fault rupture, respectively.

Figure 6: Distribution of PGA and 0.2-s and 1.0-s SA, together with their standard deviation, for the 1889 Chilik earthquake. The mean ground motions and their standard deviations have been computed from 1000 scenarios. The white star indicates the city of Almaty. The white dot and the white line describe the epicenter and the fault rupture, respectively.

Figure 7: Distribution of PGA and 0.2-s and 1.0-s SA, together with their standard deviation, for the 1887 Verny earthquake. The mean ground motions and their standard deviations have been computed from 1000 scenarios. The white star indicates the city of Almaty. The white dot and the white line describe the epicenter and the fault rupture, respectively.

Figure 8: Distribution of MSK-64 intensity for: (a) the 1911 Chon-Kemin earthquake; (b) the 1889 Chilik earthquake; and (c) the 1887 Verny earthquakes. The white star indicates the city of Almaty. The white dot and the white line describe the epicenter and the fault rupture, respectively.

Figure 9: Results of the sensitivity analysis for the 1911 Chon-Kemin earthquake using the input parameters listed in Table 2. The ground motion parameters are computed for a site in Almaty.

Figure 10: Seismic source model used in this study. The star denotes the site used for PSHA.

Figure 11: Activity rates and b-values for the individual zones in the source model. The top left map shows the earthquake catalogue within the completeness thresholds set out in Table 8 and the source zone model. The four maps below show the activity rate (first row) and the b-value (bottom row) of each source zone, together with the standard deviation (maps on the right). The white star denotes the site.

Figure 12: Magnitude-frequency recurrence for the source zone NISK.

Figure 13: Seismic hazard curves for a site in Almaty. The estimated ground motion values, together with their error-bars, for the scenario earthquakes are indicated by the circles.

Figure 14: Disaggregation by magnitude Mw, Joyner-Boore distance and epsilon ε for two pairs of 0.2-s SA values and return periods: (a) 0.48 ± 0.17 g and 122 ± 72 yr.; and (b) 1.11 ± 0.44 g and 555 ± 517 yr.

Figure 15: Disaggregation by magnitude Mw, Joyner-Boore distance and epsilon ε for two pairs of 1.0-s SA values and return periods: (a) 0.171 ± 0.069 g and 152 ± 97 yr.; and (b) 0.32 ± 0.14 g and 435 ± 373 yr.

Figure 16: Disaggregation by magnitude Mw, Joyner-Boore distance and epsilon ε for MSK-64 intensity VIII ± I and the return period of 156 ± 500 yr.

Table 1: Reference rupture model of the scenario earthquakes.

	1911 Chon-Kemin	**1889 Chilik**	**1887 Verny**
Epicenter	42.80 ± 0.28† °N, 77.30 ± 0.49† °E	43.17 ± 0.50§ °N, 78.55 ± 0.50§ °E	43.10°N, 76.80°E
Mw	8.0 ± 0.1†	8.2 ± 0.2‡	7.3 ± 0.2‡
Dip [°]	52 ± 10†	70	60
Rake [°]	98 ± 10†	120	98
Depth [km]	20 ± 3†	40	20
Rupture length [km]	202 ± 28*	260 ± 71*	75 ± 20*
Down-dip width [km]	50 ± 5*	42	31 ± 8*

*The standard deviation is estimated from the propagation of statistical errors.

†The standard deviation is from Kulikova and Krüger (2015).

‡ The standard deviation is from Scordilis (2006).

§ The standard deviation is reported in Bindi et al. (2014).

Table 2: PGA, 0.2-s and 1.0-s SA, and MSK-64 intensity in Almaty for the scenario earthquakes.

	1911 Chon-Kemin	**1889 Chilik**	**1887 Verny**
PGA [g]	0.230 ± 0.076	0.166 ± 0.056	0.49 ± 0.19
SA(0.2 s) [g]	0.48 ± 0.17	0.34 ± 0.12	1.11 ± 0.44
SA(1.0 s) [g]	0.171 ± 0.069	0.138 ± 0.060	0.32 ± 0.14
MSK-64	VIII ± I	VIII ± I	VIII ± I

Table 3: Sensitivity analysis of the ground shaking scenario for the 1911 Chon-Kemin earthquake*.

# Test		**PGA ± σ [g]**	**0.2-s SA ± σ [g]**	**1.0-s SA ± σ [g]**
1 - Site conditions	Soft rock	0.272 ± 0.089	0.59 ± 0.20	0.248 ± 0.098
2 - GMPE	Boore et al. (2014)	0.227 ± 0.072	0.47 ± 0.15	0.168 ± 0.061
3 - GMPE	Chiou and Youngs (2008)	0.234 ± 0.070	0.52 ±0.17	0.151 ± 0.055
4 - GMPE	Akkar et al. (2014)	0.228 ± 0.085	0.45 ± 0.18	0.194 ± 0.080
5 - Epicenter	42.99°N, 78.37°E	0.230 ± 0.076	0.48 ± 0.17	0.171 ±0.069
6 - Focal mechanism	Dip = 45°	0.32 ± 0.11	0.69 ± 0.25	0.230 ± 0.095
7 - Focal mechanism	Oblique, dip = 65°	0.147 ± 0.051	0.30 ± 0.11	0.121 ±0.055
8 - Multi-segmented rupture	Varying dips	0.188 ± 0.063	0.39 ± 0.14	0.143 ± 0.059

*The second column indicates the parameter changed in each test; and the third, fourth and fifth columns show the estimate of ground motion parameter for the site in Almaty.

Table 4: Maximum magnitude (Mmax) distribution for the source model.

	Mmax1	**Weight 1**	**Mmax2**	**Weight 2**	**Mmax3**	**Weight 3**	**Mmax4**	**Weight 4**
ALAI	7.5	0.20	8.0	0.60	8.2	0.20	-	-
ATBA	7.0	0.25	7.5	0.25	8.0	0.25	8.2	0.25
CTS1	8.2	0.40	8.3	0.40	8.5	0.20	-	-
JUNG	8.2	0.40	8.3	0.40	8.5	0.20	-	-
FERR	7.5	0.20	8.0	0.60	8.2	0.20	-	-
FTS1	8.2	0.40	8.3	0.40	8.5	0.20	-	-
FTS2	8.2	0.40	8.3	0.40	8.5	0.20	-	-
FTS3	8.2	0.40	8.3	0.40	8.5	0.20	-	-
KERS	7.0	0.25	7.5	0.25	8.0	0.25	8.2	0.25
KZPL	6.5	0.25	7.0	0.25	7.5	0.25	8.0	0.25
KYRG	8.2	0.40	8.3	0.40	8.5	0.20	-	-
NARY	7.0	0.25	7.5	0.25	8.0	0.25	8.2	0.25
NISK	8.2	0.40	8.3	0.40	8.5	0.20	-	-
SISK	7.0	0.25	7.5	0.25	8.0	0.25	8.2	0.25
SUUS	8.2	0.40	8.3	0.40	8.5	0.20	-	-
YILI	8.2	0.40	8.3	0.40	8.5	0.20	-	-
CKCF	8.2	0.40	8.3	0.40	8.5	0.20	-	-
TFF	8.2	0.40	8.3	0.40	8.5	0.20	-	-

Table 5: Focal depth (h) distribution for the source model.

	h1 [km]	Weight 1	h2 [km]	Weight 2	h3 [km]	Weight 3	h4 [km]	Weight 4	h5 [km]	Weight 5	h6 [km]	Weight 6
ALAI	5	0.10	10	0.20	15	0.25	20	0.25	25	0.20	-	-
ATBA	5	0.10	10	0.20	15	0.25	20	0.25	25	0.20	-	-
CTS1	10	0.30	20	0.30	30	0.20	40	0.20	-	-	-	-
CTS2	10	0.30	20	0.30	30	0.20	40	0.20	-	-	-	-
FERR	5	0.10	10	0.20	15	0.25	20	0.25	25	0.20	-	-
FTS1	10	0.25	20	0.25	30	0.25	40	0.10				
FTS2	10	0.25	20	0.25	30	0.25	40	0.10				
FTS3	10	0.25	20	0.25	30	0.25	40	0.10				
KERS	5	0.10	10	0.20	15	0.25	20	0.25	25	0.20	-	-
KZPL	10	0.30	20	0.30	30	0.20	40	0.20	-	-	-	-
KYRG	5	0.10	10	0.20	15	0.25	20	0.25	25	0.20	-	-
NARY	5	0.10	10	0.20	15	0.25	20	0.25	25	0.20	-	-
NISK	10	0.15	15	0.30	20	0.30	25	0.15	30	0.05	40	0.05
SISK	5	0.10	10	0.20	15	0.25	20	0.25	25	0.20	-	-
SUUS	5	0.10	10	0.20	15	0.25	20	0.25	25	0.20	-	-
YILI	10	0.30	20	0.30	30	0.20	40	0.20	-	-	-	-
CKCF	10	0.20	15	0.20	20	0.30	25	0.30	-	-	-	-
TFF	10	0.20	15	0.20	20	0.30	25	0.30	-	-	-	-

Table 6: Return periods of the ground motion values for a site in Almaty for the scenario earthquakes.

	PGA [g]	**Return period [years]**	**0.2-s SA [g]**	**Return period [years]**	**1.0-s SA [g]**	**Return period [years]**	**MSK-64**	**Return period [years]**
1911 Chon-Kemin	0.230 ± 0.076	133 ± 77	0.48 ± 0.17	125 ± 72	0.171 ± 0.069	159 ± 102	VIII ± I	161 ± 483
1889 Chilik	0.166 ± 0.056	78 ± 42	0.34 ± 0.12	74 ± 38	0.138 ± 0.060	115 ± 74	VIII ± I	161 ± 483
1887 Verny	0.49 ± 0.19	556 ± 519	1.11 ± 0.44	556 ± 447	0.32 ± 0.14	455 ± 369	VIII ± I	161 ± 483

Table 7: Hierarchy of magnitude selected among the available magnitude estimates in the ISC database.

	Magnitude	Agency
1	Mw	Global Centroid Moment Tensor
2	Mw	National Earthquake Information Centre
3	Ms	International Seismological Centre
4	mb	International Seismological Centre
5	Ms	National Earthquake Information Centre
6	mb	National Earthquake Information Centre
7	Ms	International Data Centre for Comprehensive Nuclear-Test-Ban Treaty Organization
8	mb	International Data Centre for Comprehensive Nuclear-Test-Ban Treaty Organization
9	Ms	European-Mediterranean Seismological Centre
10	mb	European-Mediterranean Seismological Centre
11	Ms/mb	Agency providing the hypocentral location

Table 8: Completeness periods for the catalogue.

Mw	Complete since
4.5	1970
5.0	1965
5.5	1925
6.0	1875
6.5	1875
7.0	1875
7.5	1875
8.0	1875

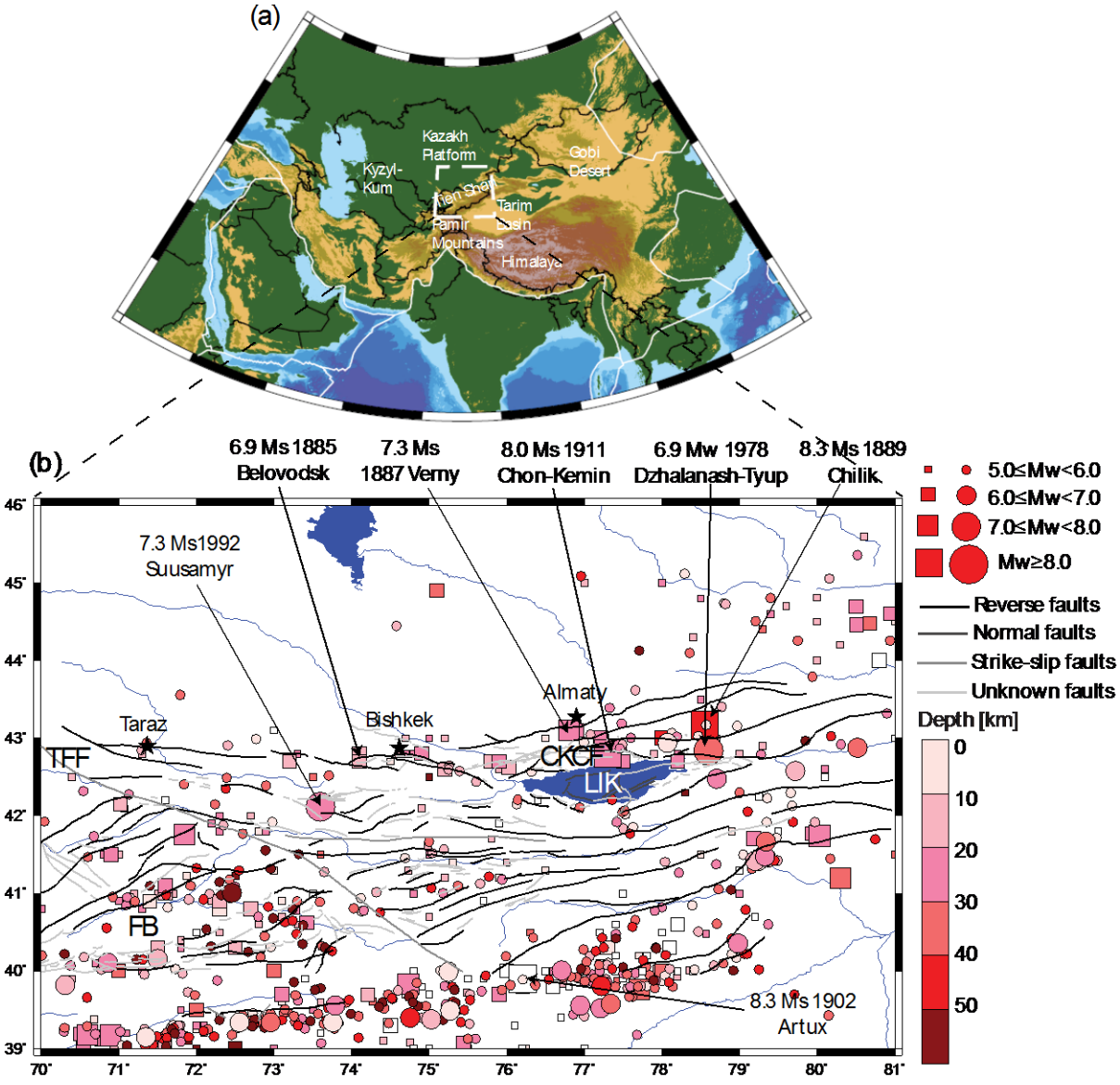
(a)
Kazakh Platform
Kyzyl-Kum
Tien Shan
Tarim Basin
Pamir Mountains
Gobi Desert
Himalaya
(b)
6.9 Ms 1885 Belovodsk
7.3 Ms 1887 Verny
8.0 Ms 1911 Chon-Kemin
6.9 Mw 1978 Dzhalanash-Tyup
8.3 Ms 1889 Chilik
7.3 Ms1992 Suusamyr
Taraz
Bishkek
Almaty
TFF
CKF
LIK
FB
8.3 Ms 1902 Artux
5.0≤Mw<6.0
6.0≤Mw<7.0
7.0≤Mw<8.0
Mw≥8.0
Reverse faults
Normal faults
Strike-slip faults
Unknown faults
Depth [km]
0
10
20
30
40
50
46°
45°
44°
43°
42°
41°
40°
39°
70°
71°
72°
73°
74°
75°
76°
77°
78°
79°
80°
81°

Figure 1

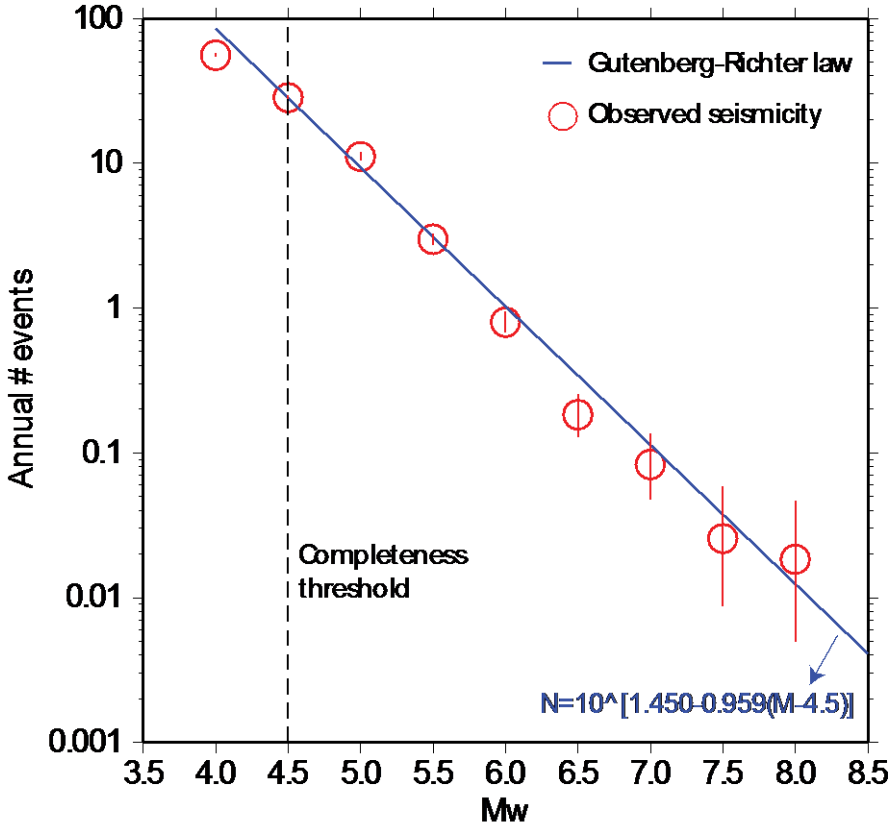

1322

1323 **Figure 2**

1324

1325

1326

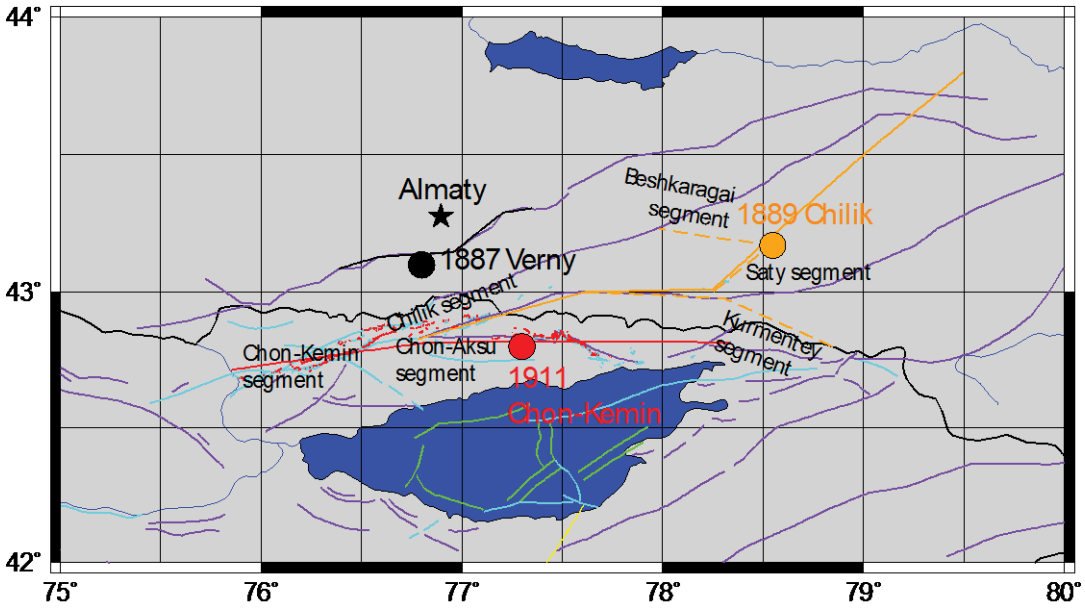
44°
43°
42°
75°
76°
77°
78°
79°
80°
Almaty
1887 Verny
Beshkaragai segment
1889 Chilik
Saty segment
Chilik segment
Kurmenty segment
Chon-Kemin segment
Chon-Aksu segment
1911 Chon-Kemin

Figure 3

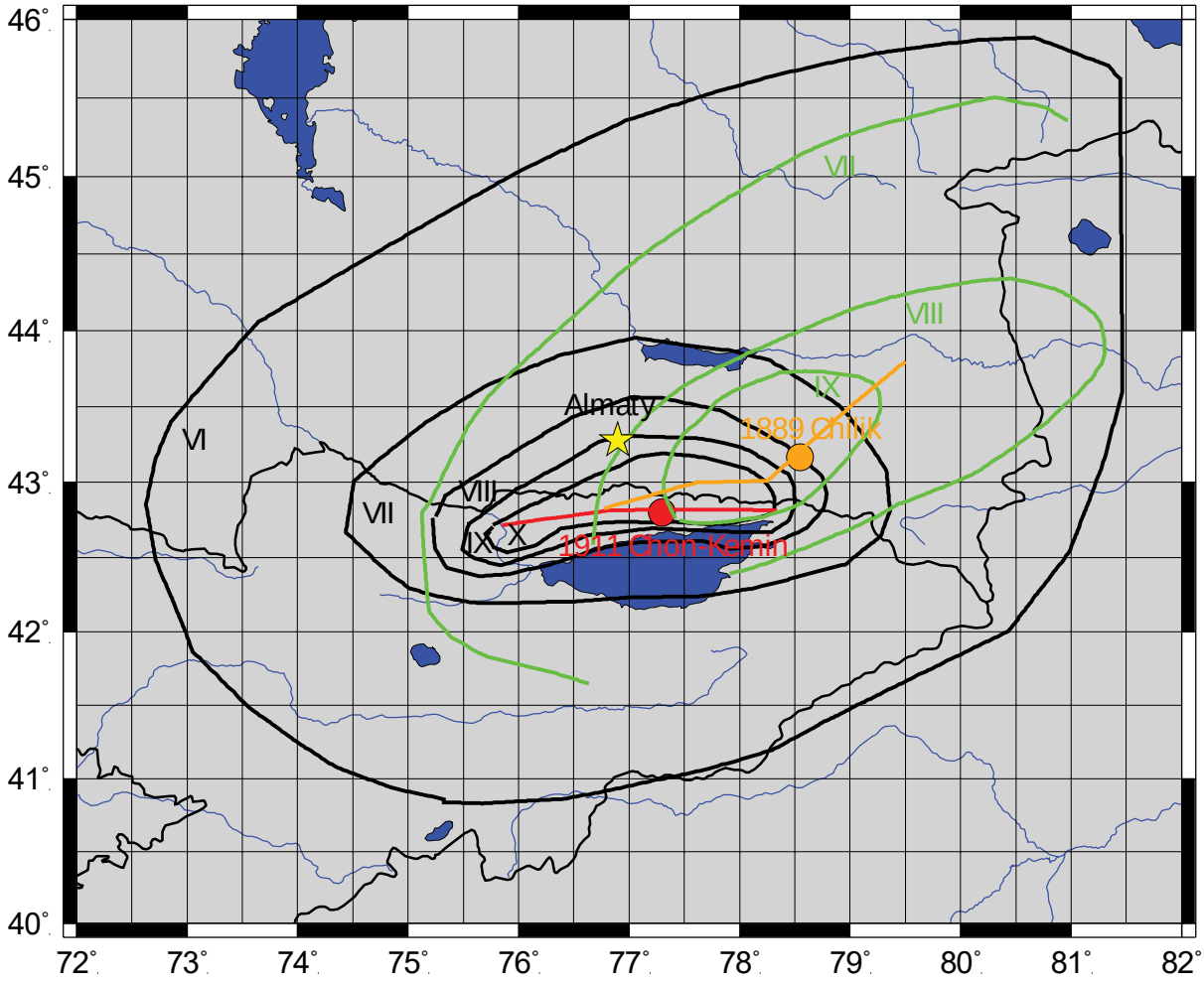

1331

1332 **Figure 4**

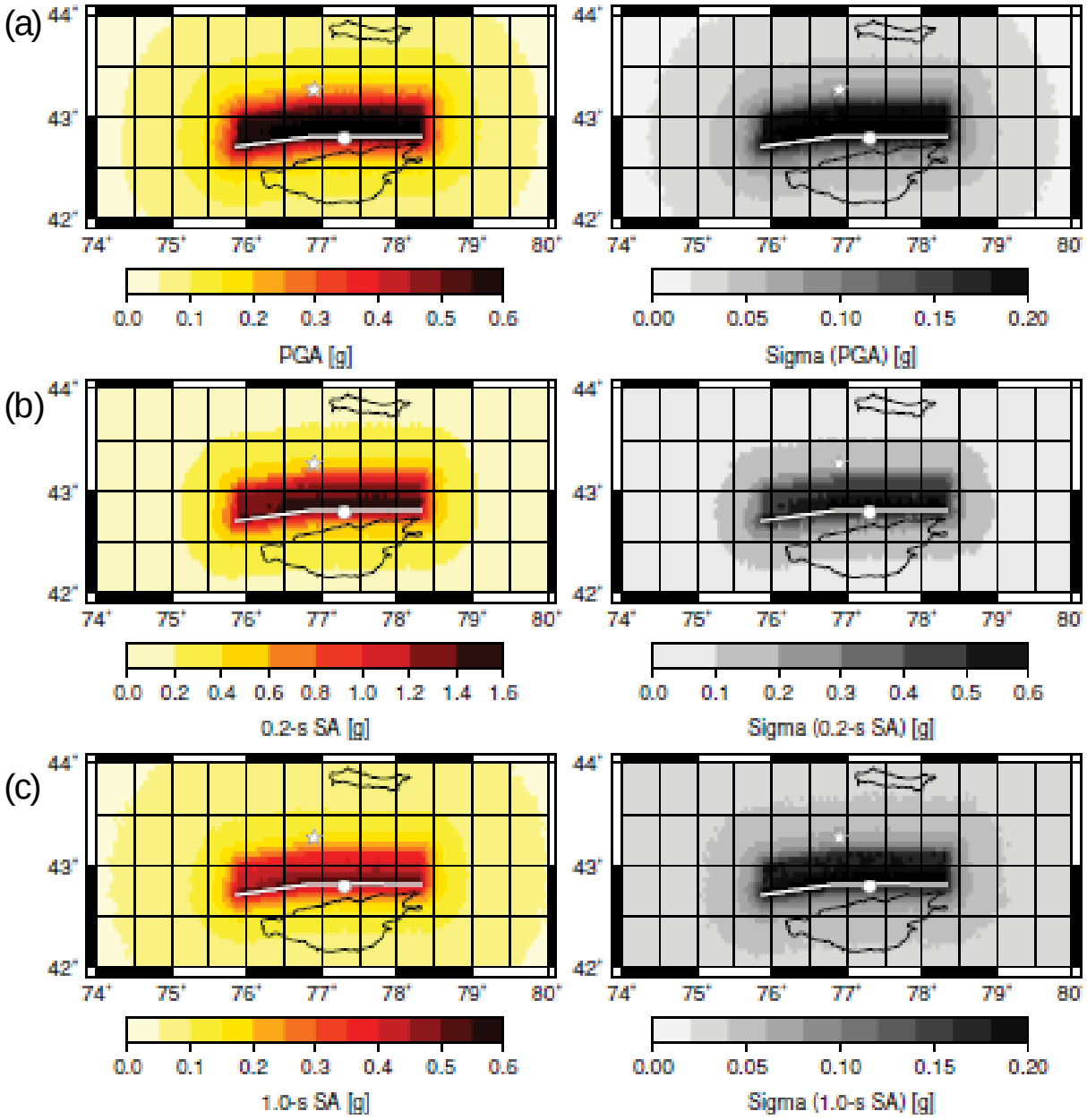

1333

1334 **Figure 5**

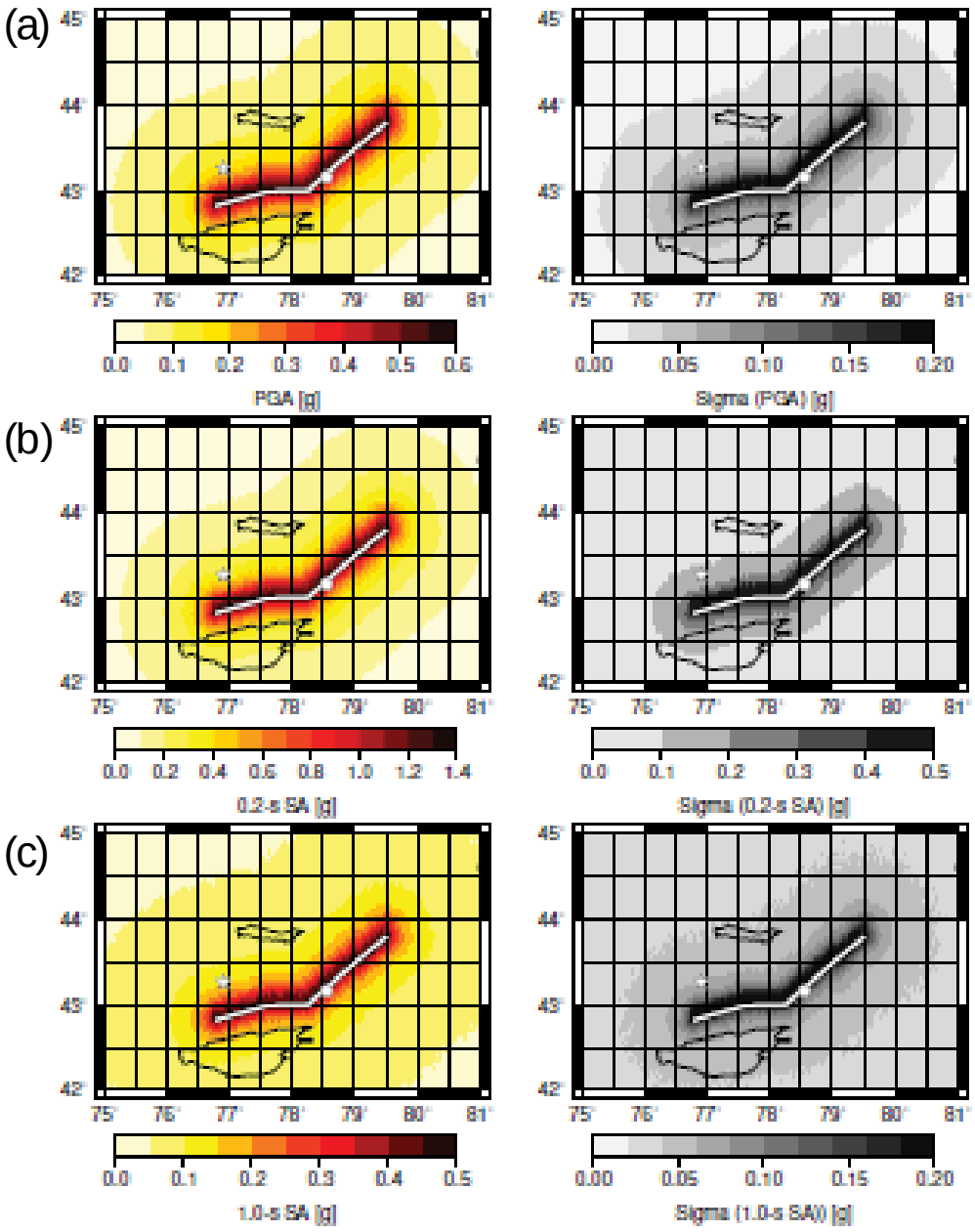

1335

1336 **Figure 6**

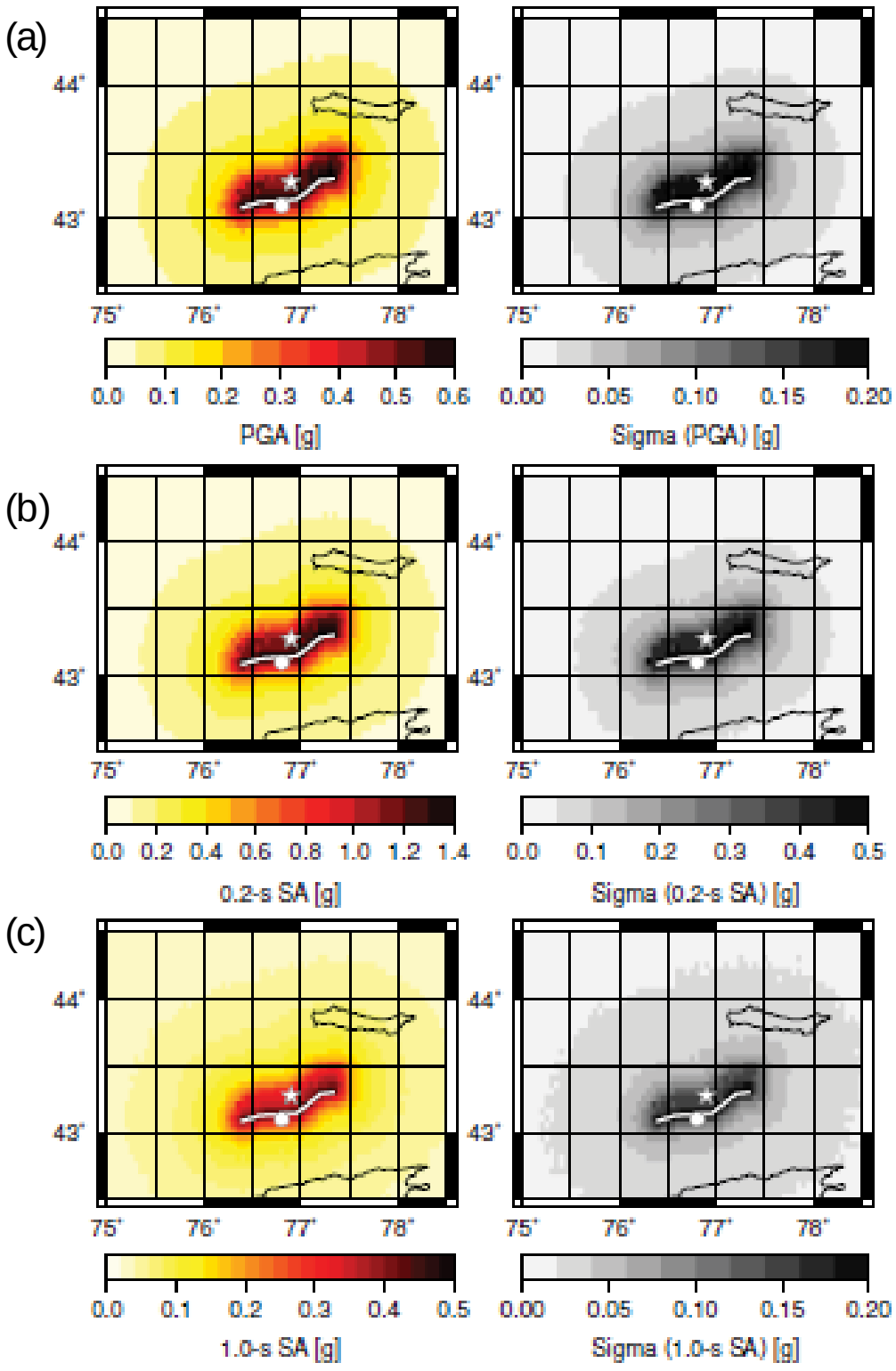
(a)
44°
43°
75°
76°
77°
78°
0.0 0.1 0.2 0.3 0.4 0.5 0.6
PGA [g]
0.00 0.05 0.10 0.15 0.20
Sigma (PGA) [g]
(b)
0.0 0.2 0.4 0.6 0.8 1.0 1.2 1.4
0.2-s SA [g]
0.0 0.1 0.2 0.3 0.4 0.5
Sigma (0.2-s SA) [g]
(c)
0.0 0.1 0.2 0.3 0.4 0.5
1.0-s SA [g]
0.00 0.05 0.10 0.15 0.20
Sigma (1.0-s SA) [g]

Figure 7

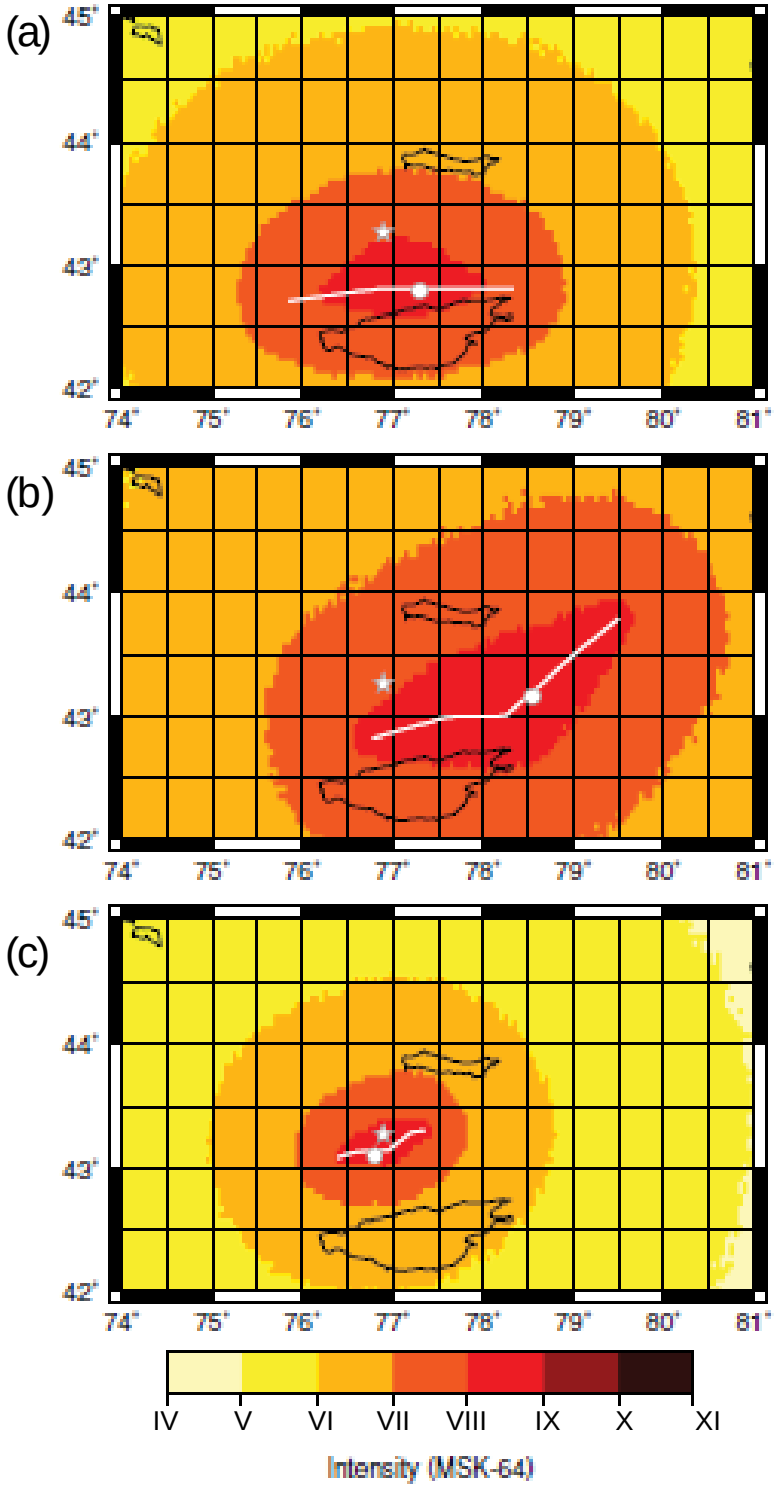

1340

1341 **Figure 8**

1342

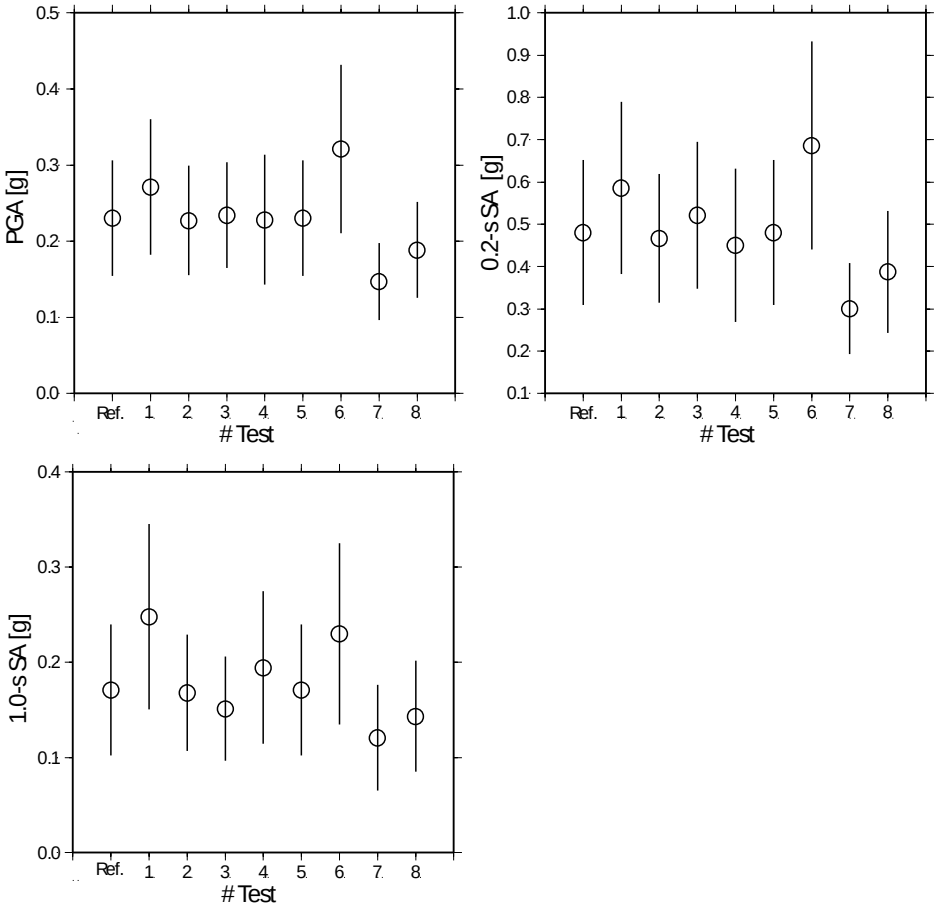

1343

1344 **Figure 9**

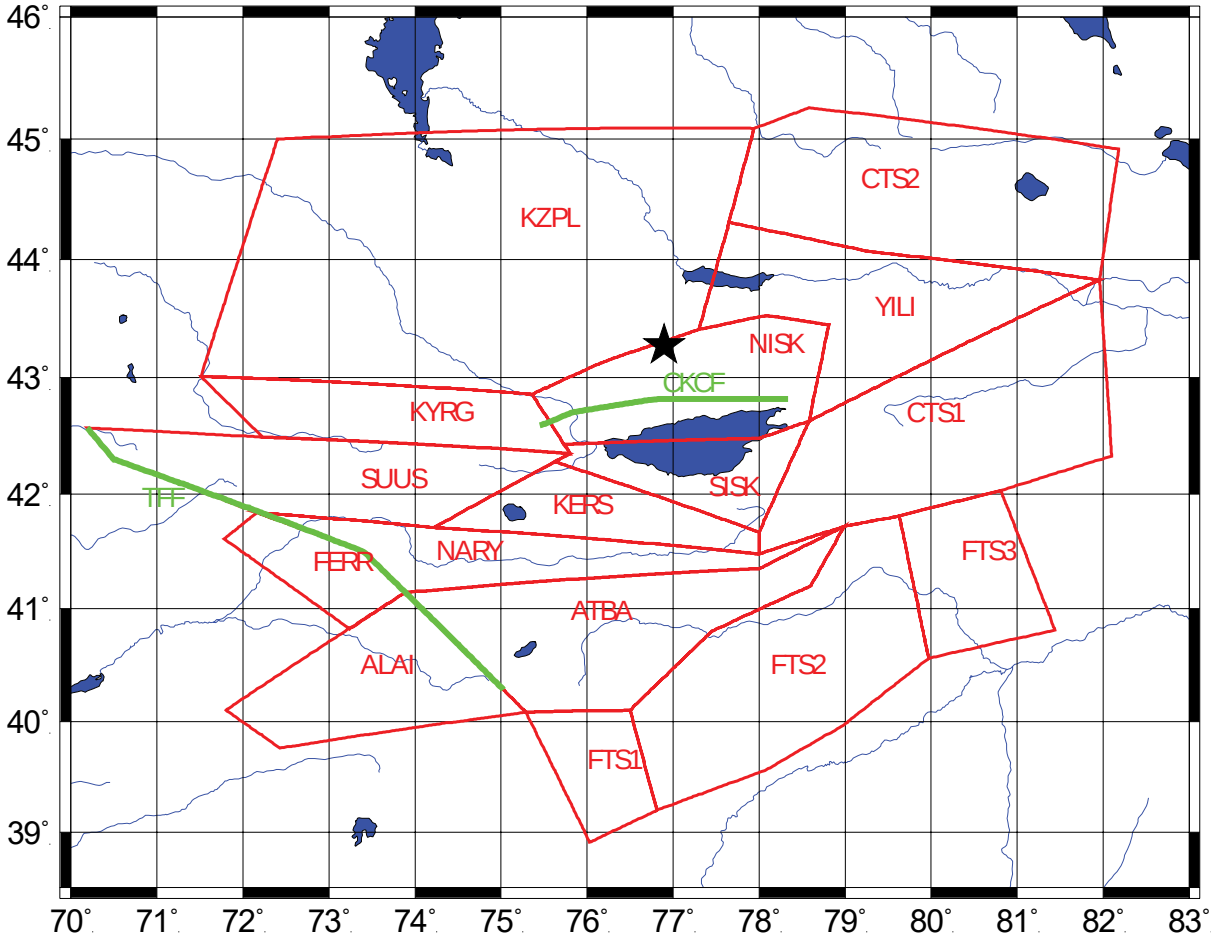
46°
45°
44°
43°
42°
41°
40°
39°
70°
71°
72°
73°
74°
75°
76°
77°
78°
79°
80°
81°
82°
83°
KZPL
CTS2
YILI
NISK
CKCF
KYRG
CTS1
SUUS
TFF
KERS
SISK
FERR
NARY
FTS3
ATBA
ALAT
FTS2
FTS1

Figure 10

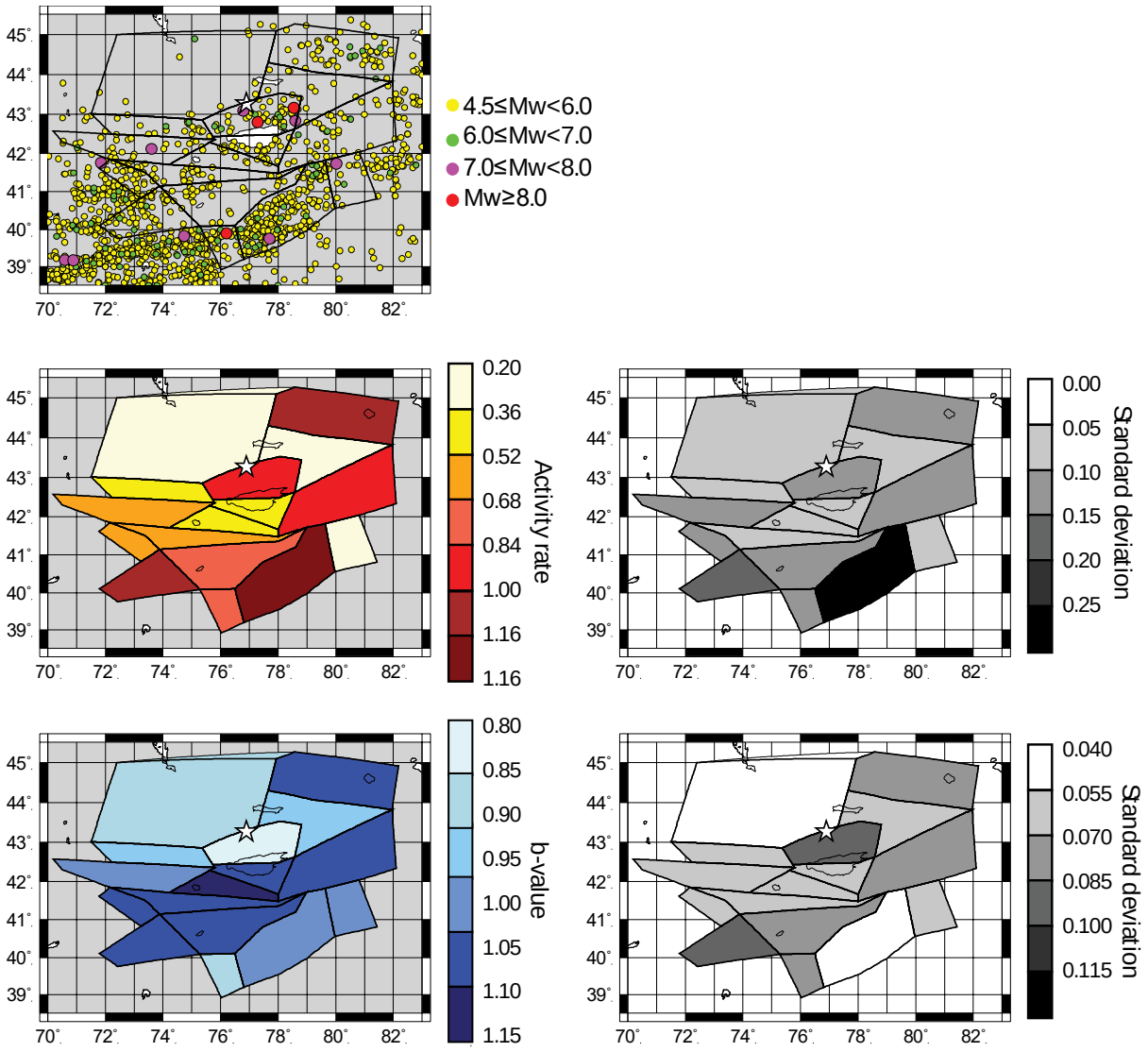
4.5≤Mw<6.0
6.0≤Mw<7.0
7.0≤Mw<8.0
Mw≥8.0
Activity rate
0.20
0.36
0.52
0.68
0.84
1.00
1.16
1.16
Standard deviation
0.00
0.05
0.10
0.15
0.20
0.25
b-value
0.80
0.85
0.90
0.95
1.00
1.05
1.10
1.15
Standard deviation
0.040
0.055
0.070
0.085
0.100
0.115
45°
44°
43°
42°
41°
40°
39°
70°
72°
74°
76°
78°
80°
82°

Figure 11

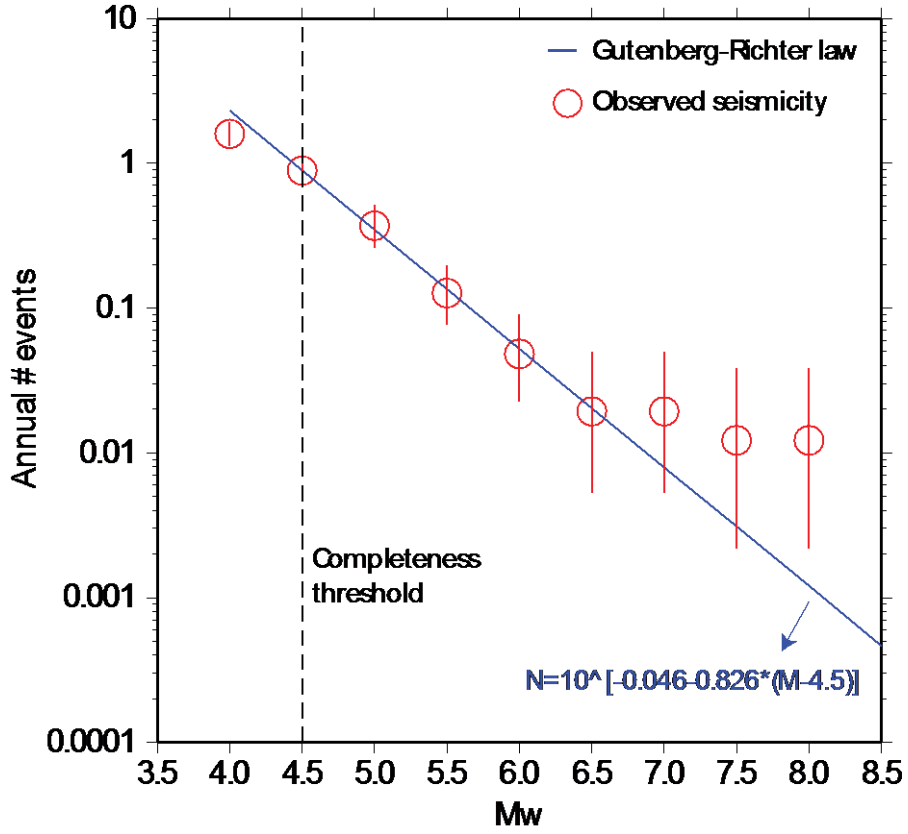

1349

1350 **Figure 12**

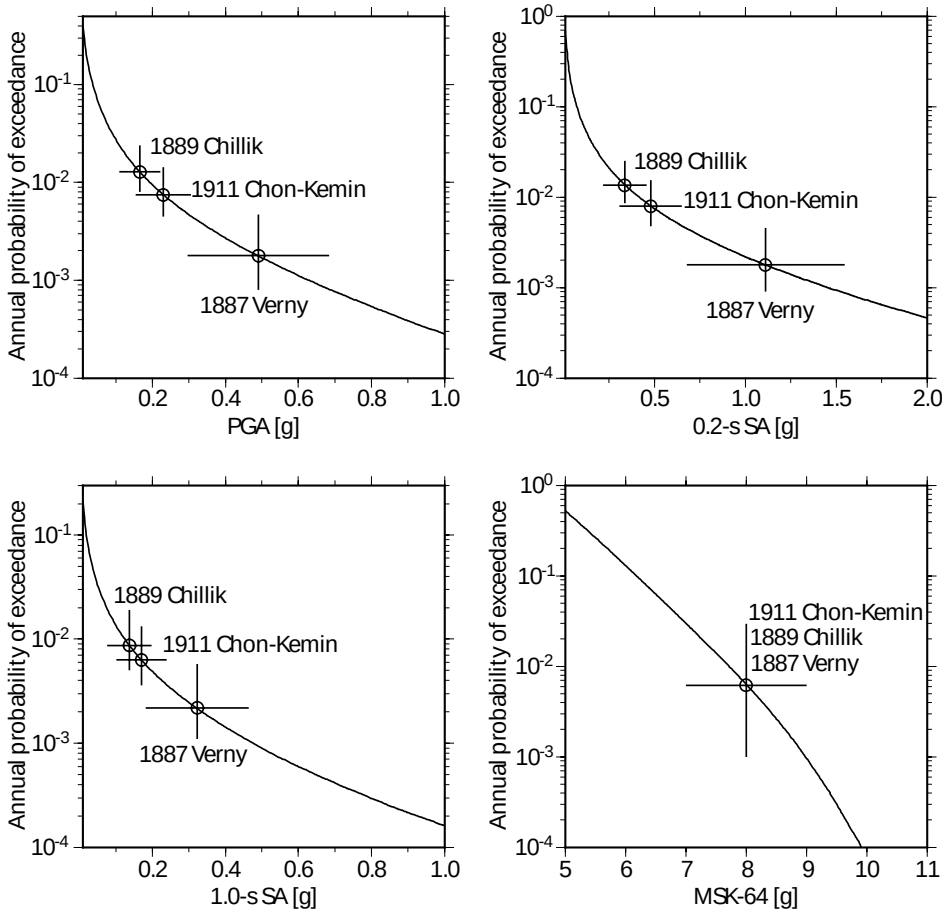

1351

1352 **Figure 13**

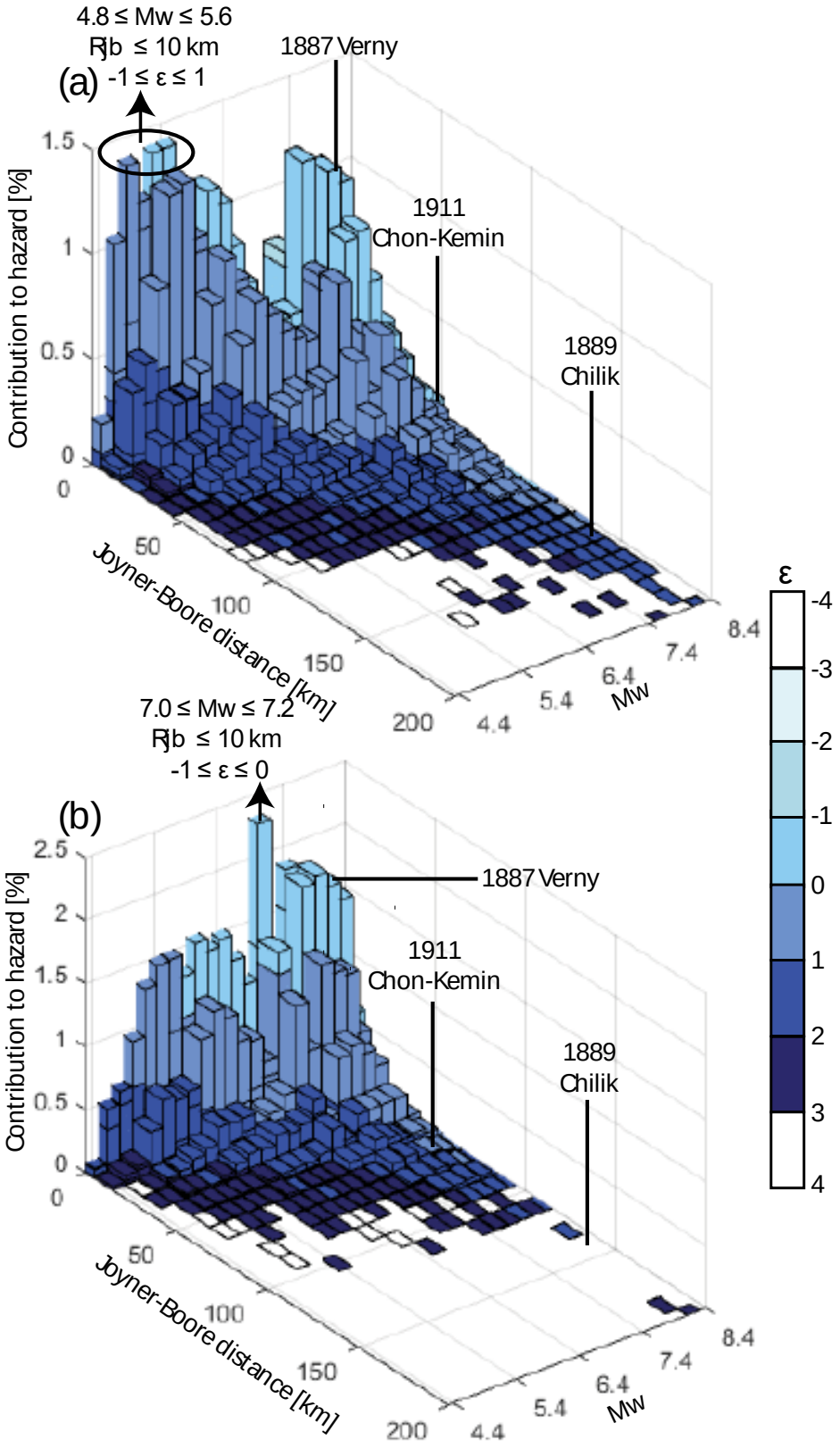

1353

1354 **Figure 14**

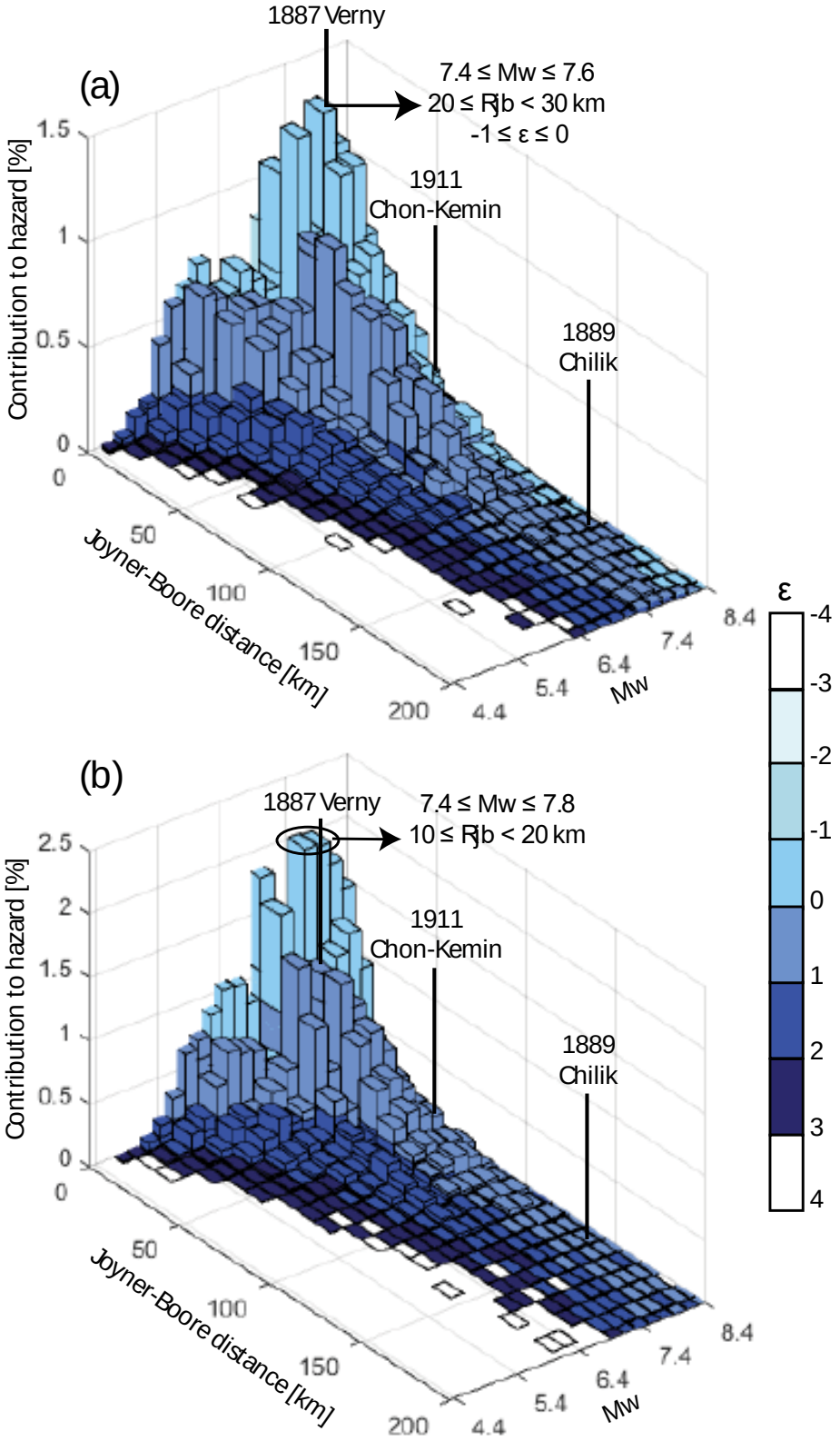

1355

1356 **Figure 15**

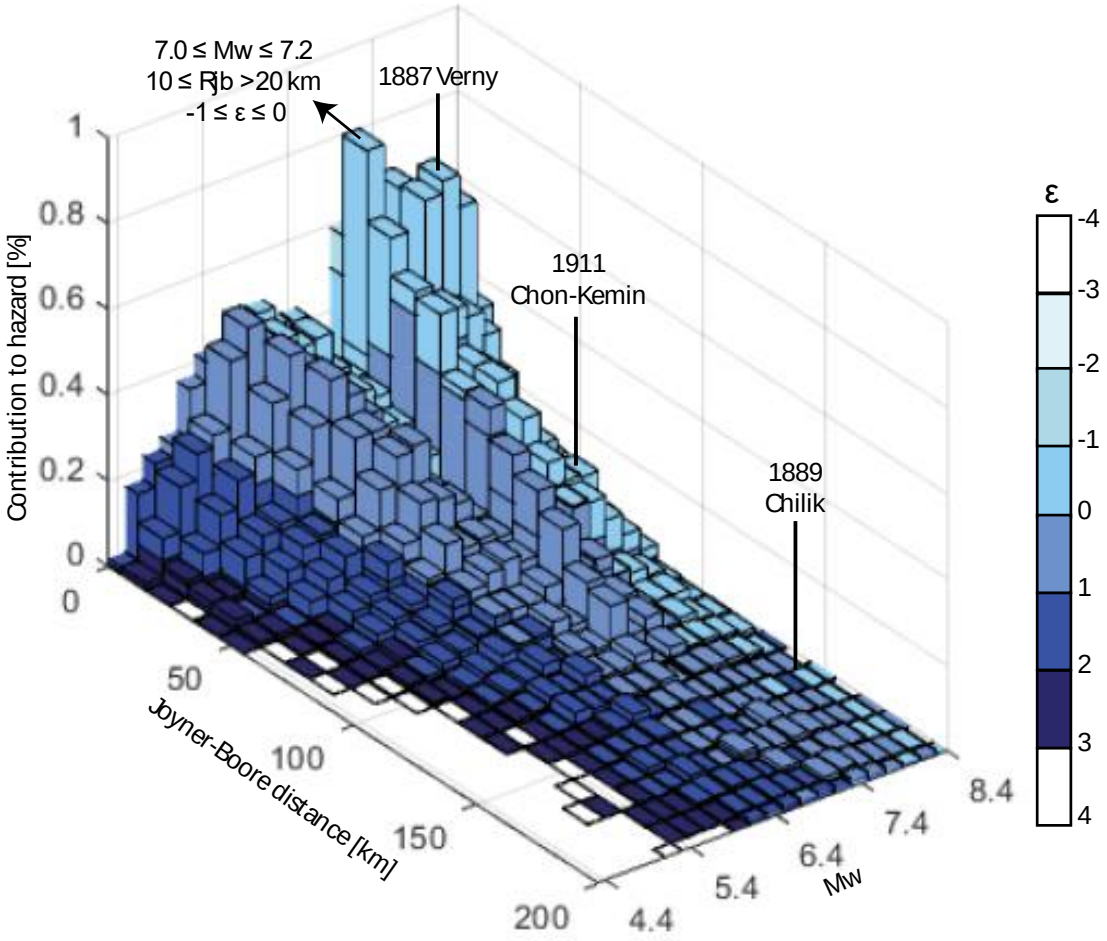

1357

1358 **Figure 16**